Control Engineering Practice 109 (2021) 104750

Contents lists available at ScienceDirect

Control Engineering Practice

journal homepage: www.elsevier.com/locate/conengprac

Stabilization of city-scale road traffic networks via macroscopic fundamental diagram-based model predictive perimeter control

Isik Ilber Sirmatel *, Nikolas Geroliminis

Urban Transport Systems Laboratory (LUTS), School of Architecture, Civil and Environmental Engineering, École Polytechnique Fédérale de Lausanne (EPFL), 1015 Lausanne, Switzerland

ARTICLE INFO

Keywords:
Traffic perimeter control
Macroscopic fundamental diagram
Model predictive control
Stabilization
Large-scale urban road networks

ABSTRACT

Traffic control for large-scale urban road networks remains a challenging problem. Aggregated dynamical models of city-scale traffic, based on the macroscopic fundamental diagram (MFD), enable development of model-based perimeter control methods. Involving actuation over aggregated traffic flows, perimeter control specifies an effective and practicable congestion control solution. In this paper, we propose nonlinear model predictive perimeter control schemes, for regulation and economic optimization objectives, with closed-loop stability by construction. Macroscopic and microscopic simulations demonstrate the performance and domain of attraction properties of the proposed formulations. Results indicate potential of the methods for efficient and reliable control of city-scale traffic.

1. Introduction

Improving mobility in city-scale urban road traffic networks presents substantial challenges in development of modeling, estimation, and control techniques. Inadequate infrastructure, lack of coordination between different parts of the network, spatiotemporal congestion propagation, the sheer size of the system, and the interactions of drivers with traffic management systems, among others, constitute the complications which arise when developing urban road network models and control schemes. Although development of real-time traffic control methods received significant attention in the literature especially in the last decades (see Bellemans et al., 2006; Dotoli et al., 2006; Ioslovich et al., 2011, and for a review see Papageorgiou et al., 2003), city-level traffic modeling and control design for heterogeneously congested networks remains a challenging problem.

Many works in the literature focused on modeling and control of urban traffic, which usually considered link-level traffic flows local control strategies (see Aboudolas et al., 2010; Diakaki et al., 2002; Kouvelas et al., 2014; Lin et al., 2011; Tettamanti et al., 2013; Varaiya, 2013; van de Weg et al., 2019; Wongpiromsarn et al., 2012). Link-level traffic models facilitate accurate simulations with high level of detail, however they might complicate control design for large scale networks due to high model complexity. Furthermore, heavily congested conditions might create problems for local control strategies as congested regions upstream are not protected. Highly detailed traffic information might be difficult to measure or estimate, further complicating their use for local controllers.

Perimeter control approach for large-scale networks appeared as a practicable and possibly complementary option to local traffic signal control methods. In perimeter control, the idea is to manipulate macroscopic traffic flows exchanged between neighborhood-sized areas (i.e., regions) of the urban network by changing the green times of the traffic lights on the boundaries (i.e., perimeters) between the regions. Feedback control systems, using the perimeter flow manipulation as actuator, can then be constructed by instrumenting the road network with traffic sensors.

Model-based control design for perimeter controlled urban networks is possible using the macroscopic fundamental diagram (MFD) of urban traffic. First proposed by Godfrey (1969) and, for large-scale urban networks, experimentally proven to exist by Geroliminis and Daganzo (2008), the MFD enables modeling of an urban region with homogeneously distributed congestion by providing a unimodal, low-scatter, and demand-insensitive relationship between accumulation and trip completion flow (Geroliminis & Daganzo, 2008).

The MFD, despite being a powerful tool for building aggregated models, might also face difficulties that can hamper its accuracy in traffic modeling. Recently, a large number of empirical studies have further investigated the physical properties and network conditions for which an MFD exists with low scatter (see Fu et al., 2020; Huang et al., 2019; Loder et al., 2019; Paipuri et al., 2020). Heterogeneously distributed congestion over the road links, for example, can lead to high scatter in the MFD (see Geroliminis & Sun, 2011). Despite the challenges, it is possible to considerably reduce traffic model complexity by using the MFD, thus enabling model-based network-level control

* Corresponding author.
E-mail address: isik.sirmatel@epfl.ch (I.I. Sirmatel).

https://doi.org/10.1016/j.conengprac.2021.104750
Received 13 August 2020; Received in revised form 4 December 2020; Accepted 19 January 2021
Available online 29 January 2021
0967-0661/© 2021 The Authors. Published by Elsevier Ltd. This is an open access article under the CC BY-NC-ND license (http://creativecommons.org/licenses/by-nc-nd/4.0/).

design with aggregated, low-dimensional dynamical models. Since the first work on MFD-based control considering a single region (see Daganzo, 2007), many methods for the analysis, modeling, and control via MFD-based traffic modeling have been proposed: Proportional–integral control (Aboudolas & Geroliminis, 2013; Ding et al., 2017; Ingole et al., 2020; Keyvan-Ekbatani et al., 2012, 2015a), optimal control (Aalipour et al., 2018; Haddad, 2017a, 2017b), robust control (Ampountolas et al., 2017; Haddad, 2015; Haddad & Shraiber, 2014; Mohajerpoor et al., 2020; Zhong et al., 2018a), adaptive control (Haddad & Mirkin, 2016; Haddad & Zheng, 2018; Kouvelas et al., 2017a), control with route choice (Menelaou et al., 2017, 2018), hierarchical control (Fu et al., 2017).

Enabled via MFD-based modeling approaches, model predictive traffic control methods also received increasing interest: MPC with MFD-based travel time and delays as performance measures (Csikós et al., 2017), convex formulation of the optimal perimeter control problem yielding linear MPC (Kouvelas et al., 2017b), two-level hierarchical MPC with MFD-based and link-level models (Zhou et al., 2017), multimodal MFDs network model-based MPC of city-scale ride-sourcing systems (Ramezani & Nourinejad, 2018), MPC with perimeter control and regional route guidance (Sirmatel & Geroliminis, 2018) and extensions with a path assignment mechanism (Yildirimoglu et al., 2018), multi-scale stochastic MPC considering conventional and connected vehicles (Yang et al., 2018), combined operation of state estimation and MPC (Sirmatel & Geroliminis, 2019). Detailed literature reviews of MFD-based modeling and control can be found in Haddad (2017a) and Sirmatel and Geroliminis (2019).

Closed-loop stability of MFD-based perimeter control schemes received relatively modest attention in the literature. In the first work explicitly discussing stability of MFD-based control, Haddad and Geroliminis (2012) consider a two-state two-region MFDs system and formulate an optimal control for maximizing total trip completion. They further develop an algorithm for constructing the boundaries of the domain of attraction both numerically and analytically, and design a state-feedback controller for stabilizing the system and regulating it to a given equilibrium point. The domains of attraction for a three-state two-region MFDs system under closed-loop with the state-feedback controller are constructed numerically via macroscopic simulations. In Haddad and Shraiber (2014) first a linear model of a two-state one-region MFD system is derived by introducing uncertain parameters for the split ratio and linearization of the MFDs around a given setpoint (split ratio is the ratio of vehicles in a region with a certain destination to all vehicles in the region). A robustly stabilizing proportional–integral controller is then designed, using methods from quantitative feedback theory, against uncertainty in the split ratio and the MFD. The proposed controller is tested in macroscopic simulations with various levels of inflow demand and errors in the MFDs. Results include comparisons with an MPC controller, however no discussions of either its closed-loop stability properties or the domains of attraction of the proposed controllers are included. The methods proposed in Haddad and Shraiber (2014) are extended in Haddad (2015) by considering a multi-region MFDs system model and control input constraints. The MFDs are linearized around a set point, and the split ratios and MFD slopes are formulated as uncertain parameters, yielding an uncertain linear system. A robustly stabilizing controller to regulate the system to an equilibrium under bounded disturbances is then designed using the interpolation-based control approach (see Nguyen et al., 2013). Results considering a control design using a two-state two-region MFDs system model are presented, with various macroscopic simulation scenarios involving different initial accumulation states and levels of inflow demands, comparing the proposed controller with a robust state feedback controller designed via LMI and a nominal linear MPC controller. One-, two-, and multi-regions MFDs system models are considered in Zhong et al. (2018b), establishing connections between MFDs system boundary conditions, inflow demand levels, and existence of equilibrium points. The work also includes stability analysis for an uncontrolled one-state one-region MFD system, together with calculation of feasible inflow demands yielding equilibrium. The results contain various traffic scenarios considering MFDs systems with different number of regions, comparing an uncontrolled case with a proportional controller. In Zhong et al. (2018a) a two-state two-region MFDs system model is used to design a robust continuous-time control Lyapunov function (CLF) based controller, and operation of the controller is demonstrated via macroscopic simulations considering various inflow demand trajectories and control input bounds. Perimeter control systems can only operate via updating the control inputs at the beginning of each traffic light cycle, and since these cycles are of considerable length (e.g., 60 s or more), the discrete-time nature of perimeter control implementation should not be neglected. However the study in Zhong et al. (2018a) does not examine how well the proposed continuous-time CLF-based controller would work in such a discrete-time setting.

In spite of the aforementioned works examining stability of MFDs systems and many other works mentioned in the previous paragraphs focusing on MPC of perimeter controlled MFDs systems, closed-loop stability of model predictive perimeter control remains unexplored. To address this issue we propose nonlinear MPC schemes for the regulation and economic optimization objectives for MFD-based perimeter control with closed-loop stability by construction. To serve as a non-predictive benchmark controller, a discrete-time CLF-based controller is also proposed. The proposed methods enable stabilization and congestion control in city-scale urban road traffic networks. Such large scale systems are difficult to model and control via conventional link-level methods due the sheer physical size and resulting exceedingly high dimensional models. By controlling only a subset of traffic lights, the perimeter flow actuation method (i.e., perimeter control) is capable of effective actuation of aggregated traffic flows between neighborhood-scale areas (i.e., regions). Considering aggregated traffic dynamics via macroscopic fundamental diagram yields control-oriented dynamical models in low dimensions enabling development of model-based control and estimation methods. Straightforward field implementation of such advanced city traffic control systems are made possible by integrating the perimeter flow actuators and the predictive controllers with real-time measurements from loop detectors dispersed over the controlled areas and at the region boundaries. The proposed methods, facilitating stabilization and efficient congestion recovery for city-scale networks, are shown to have strong potential for practice via extensive aggregated (macroscopic) and detailed (microscopic) simulations, examining the performance and domain of attraction properties of the controllers. Microscopic simulations involve a realistic representation of downtown Barcelona, containing more than 600 traffic lights and 1500 road links carrying traffic of tens of thousands of vehicles, highlight the field implementation potential of the proposed control methods for improving efficiency and reliability of city-scale urban road traffic.

2. Modeling

Consider a city-scale road traffic network, consisting possibly of hundreds of links and intersections carrying the traffic of thousands of vehicles, with heterogeneous distribution of congestion on its links. Using the MFD, it is possible to express the rate of vehicles exiting traffic in a neighborhood-sized area (i.e., a region) of the network as a function of the number of vehicles (i.e., accumulation) in the region. Note that a vehicle can exit the traffic in a region either through ending the trip inside the region or transferring to an adjacent region. Clustering algorithms developed for such large-scale road networks can be used to partition the network into a set of regions to obtain low intraregional heterogeneity of accumulation (see Saeedmanesh & Geroliminis, 2016). A homogeneous distribution of congestion in the resulting set of regions leads to a regional MFD that is well-defined, i.e., a low scatter of flows is observed for the same accumulation. Empirical results indicate that the MFD can be approximated by an

asymmetric unimodal curve skewed to the right, which can, for example, be chosen as a third degree polynomial (the methods in this work are not restricted by the functional form of the MFD):

$$g_i(x_i) = a_i x_i^3 + b_i x_i^2 + c_i x_i, \tag{1}$$

where x_i (vehicles; abbreviated henceforth as veh) is the accumulation of region i, $g_i(x_i)$ (veh/s) is the trip completion flow of the region (i.e., rate of vehicles exiting traffic), whereas a_i, b_i, and c_i are MFD parameters.

Consider a network consisting of a set of regions $\mathcal{R} = \{1, 2, \dots, R\}$, where $\mathcal{R}$ is the set containing the index of each region while R is the number of regions in the network. Associating each region with a well-defined MFD, aggregated dynamical models of large-scale road traffic networks can be developed based on interregional traffic flows via following vehicle conservation equations (Ramezani et al., 2015):

$$\dot{x}_{ii}(\tau) = d_{ii}(\tau) - m_{ii}(\tau) + \sum_{h \in \mathcal{N}_i} u_{hi}(\tau) m_{hii}(\tau) \tag{2a}$$

$$\dot{x}_{ij}(\tau) = d_{ij}(\tau) - \sum_{h \in \mathcal{N}_i} u_{ih}(\tau) m_{ihj}(\tau) + \sum_{h \in \mathcal{N}_i; h \neq j} u_{hi}(\tau) m_{hij}(\tau), \tag{2b}$$

where $\tau \in \mathbb{R}_{\geq 0}$ is the real time, $x_{ii} \in \mathbb{R}$ (veh) and $x_{ij} \in \mathbb{R}$ (veh) are state variables expressing the accumulation in region i with destination region i and j, respectively (with $x_i = \sum_{j=1}^{R} x_{ij}$), $d_{ii} \in \mathbb{R}$ (veh/s) and $d_{ij} \in \mathbb{R}$ (veh/s) are (possibly measured) disturbances expressing the rate of vehicles appearing in region i demanding trips to destination region i and j, respectively, $u_{ih} \in [\underline{u}, \bar{u}] \subset \mathbb{R}$ (with $0 \leq \underline{u} < \bar{u} \leq 1$) are control inputs expressing actions of perimeter control actuators between each pair of adjacent regions i and h (with $h \in \mathcal{N}_i$; where $\mathcal{N}_i$ is the set of regions adjacent to i) that can manipulate vehicle flows transferring between the regions, m_{ihj} (veh/s) is the vehicle flow attempting to transfer from i to h with destination j:

$$m_{ihj} \triangleq \theta_{ihj} \frac{x_{ij}}{x_i} g_i(x_i), \tag{3}$$

where $\theta_{ihj} \in [0, 1] \subset \mathbb{R}$ is the route choice term expressing, for the vehicles exiting region i with destination j, the ratio that is transferring to region h (with m_{hii} and m_{hij} defined similarly), whereas m_{ii} (veh/s) is the exit (i.e., internal trip completion) flow of region i:

$$m_{ii} \triangleq \frac{x_{ii}}{x_i} g_i(x_i). \tag{4}$$

Recently, several authors introduced the so-called trip based model as an alternative description of congestion dynamics (see Arnott, 2013; Batista & Leclercq, 2019; Daganzo & Lehe, 2015; Lamotte & Geroliminis, 2018; Leclercq & Paipuri, 2019). Based on the speed MFD, such models avoid the steady-state approximation between outflow and production. Trip-based models are computationally more demanding than accumulation-based models using a production-over-trip-length (PL) approximation for outflow MFDs (such as the one used in this paper). They may cause intractability when used for model-based control methods, and they cannot be written in a compact ODE form. Yet, trip-based models also provide a sounder treatment of urban traffic propagation phenomena, avoiding some artifacts associated with PL-based models, such as the temporary reduction of experienced travel time that can follow a demand surge (see Lamotte & Geroliminis, 2016). A recent paper by Mariotte et al. (2017) contains analyses of some of these issues, however focuses primarily on the consequences of a non-stationary inflow with homogeneous trip length. Nevertheless, such models require full knowledge of the trip length distributions, and, due to the complex dynamics with a high dimensional state space, would potentially cause model-based estimation control methods using such models to suffer from excessive computational burden.

Route choice effect can be omitted in modeling if the network topology leads to a single obvious regional route choice, in which case $\theta_{ihj} = 1$ for all time for only one region $h \in \mathcal{N}_i$ for each i-j pair (with $j \neq i$). The focus in this paper is on those networks where route choice can be omitted (see Sirmatel & Geroliminis, 2018 for a study where it is included). Effects of perimeter control on queuing vehicles at the boundary is another important issue that needs consideration. Microscopic simulations have shown that perimeter control does not cause strong local boundary heterogeneity if green light duration is properly distributed by considering the capacity of intersections (see, e.g., Keyvan-Ekbatani et al., 2015b or Kouvelas et al., 2017a). There are works focusing on modeling and control of MFDs systems that also take boundary queue dynamics into account (see Haddad, 2017b and Ni & Cassidy, 2019). Extension of the methods proposed in this paper to include boundary queue models can be considered for possible future research.

The dynamics (2) can be written in a compact form in discrete time as:

$$x(t+1) = F(x(t), d(t), u(t)) \tag{5}$$

where $t \in \mathbb{N}_0$ is the sampled real time, $x \in \mathbb{R}^{n_x}$ (state) and $d \in \mathbb{R}^{n_x}$ (disturbance) are the vectors of accumulation states (i.e., x_{ii} and x_{ij}) and inflow demands (i.e., d_{ii} and d_{ij}), respectively, and $u \in \mathbb{R}^{n_u}$ (control input) is the vector of perimeter control inputs (i.e., u_{ih}).

3. Stabilizing model-based perimeter control

3.1. Congestion recovery scenario

In practice, challenging traffic scenarios for urban road networks are usually those where the demands are so high that the system does not have an equilibrium. Such scenarios are typically replicated using inflow demand trajectories that are trapezoidal in time (i.e., starts with zero or low values, rises to high values and stays there for some time, and then falls to zero or low values). Simulation-based analysis of such high demand scenarios with trapezoidal trajectories can be found in most works on feedback perimeter control (see Geroliminis et al., 2013; Ramezani et al., 2015; Sirmatel & Geroliminis, 2019). Here we consider a different traffic scenario that we term congestion recovery. This scenario facilitates use of MPC methods with stability by construction properties which require assuming existence of an equilibrium. The congestion recovery scenario can be thought of as starting from the part of the trapezoidal demand scenario where the demands returned to low values (so that an equilibrium exists), however accumulations can be high due to recent high demands. The objective of the traffic control system then is to recover the system from possibly high levels of congestion (i.e., high accumulations as initial state) and steer the system towards the equilibrium point corresponding to the low demand. Such a scenario is interesting from both the traffic engineering and control systems points of view, since successful congestion recovery from high accumulations is desirable for building high performance traffic control systems, whereas it corresponds exactly to the problem of stabilization of a constrained nonlinear system from the control systems point of view, for which there exists works yielding stability by construction for MPC formulations. Congestion recovery scenarios considering many possible starting accumulation values (as initial states) corresponds then to constructing the domain of attraction of the closed loop system. Analysis and stabilizing perimeter control design considering time-varying demand profiles is an important direction for future research.

3.2. Control tasks for feedback perimeter control

In feedback perimeter control the goal is to develop traffic control systems for efficient congestion management in large-scale urban road networks with perimeter control actuation. Although the ultimate overall objective for quantitative performance can be formalized as minimizing the total time spent (TTS) for all vehicles using the network, the objective function used in control design can be formulated in various ways. Considering the connections to traffic control, here we briefly describe the central task of stabilization alongside two control

objectives that are directly applicable to feedback perimeter control, namely regulation and economic optimization. We note here that we use the term stability purely in the control theoretical sense, i.e., closed-loop stability of the dynamical system under feedback loop with a given controller, and not specifically in the sense of traffic flow stability.

Stabilization involves imparting the closed-loop system with stability, which is a control theoretical property that can roughly be stated as the capability of the system for returning to an equilibrium from an initial state. Closed-loop stability is the most important property for a control system, as reliable and efficient operation cannot be achieved if the system is unstable. Regulation involves the standard control task of steering the state of a dynamical system from an initial state to a desired equilibrium point. Considering a constant inflow demand $d(t) = d_s$ that is small enough to yield an equilibrium (i.e., a constant feasible demand, see Zhong et al., 2018b), and the corresponding values of accumulation state and perimeter control input x_s and u_s at equilibrium (i.e., $x_s = F(x_s, d_s, u_s)$), the regulation problem can be stated as steering the system to the equilibrium point (x_s, u_s). From the traffic engineering point of view, regulation corresponds to bringing the accumulation of the urban network from an arbitrary initial (possibly highly congested) state back to operation at equilibrium. Economic optimization involves formulating the control objective to correspond directly to the desired economically optimal system operation. Economically optimal traffic network operation can be formalized via the commonly used objective function describing TTS in the network, corresponding to the stage cost $\mathbf{1}^T x$. Multiplied by the sampling time and summed over time, this stage cost yields the TTS by all vehicles in the network. We note here that economic optimization is meant in the sense of economic MPC (Rawlings & Amrit, 2009), i.e., using objective functions that are, unlike the case with regulation, not necessarily positive definite with respect to the desired equilibrium.

For MFDs systems, any steady state x_s for which the regional accumulations are less than or equal to their corresponding critical accumulations is desirable in general. Such a traffic state would mean that all regions are operating in free flow traffic conditions, which corresponds to the situation where vehicles are traveling at the free flow (i.e., maximum possible) speed. In particular, comparing two such steady state points, the one with the lower total accumulation would be desirable since it corresponds to a safer condition with lower sustained loading of the network. A secondary consideration might be to have a steady state for which the regional accumulations are similar, so that the network load is balanced. We consider here a simple approach for choosing the steady state x_s: We assume a known fixed inflow demand vector d_s that is feasible, i.e., the demand is low enough for the equation $x_s = F(x_s, d_s, u_s)$ to have a solution for a given u_s satisfying $\underline{u} \le u \le \bar{u}$. We then choose a steady-state control input u_s which is not too small, so as not to be too restrictive on traffic, and which is in the interior of the input constraints set defined by $\underline{u} \le u \le \bar{u}$ (as required by Chen & Allgöwer, 1998 and Amrit et al., 2011). Then, given these fixed values of d_s and u_s, solving $x_s = F(x_s, d_s, u_s)$ yields the steady state x_s. In practice it might be difficult to know the fixed inflow demand d_s accurately, although it can be estimated without measuring it directly, see Sirmatel and Geroliminis (2019). Furthermore, inflow demand $d(t)$ is usually time-varying, resulting also in the steady state x_s being time-varying. However the main objective in congestion recovery control is to bring the network back from highly congested conditions to an equilibrium condition instead of arriving exactly at the desired steady state x_s, thus reasonable errors in d_s and the resulting steady-state error are not critical for successful congestion recovery. Nevertheless, the case of unknown and time-varying inflow demands can be treated by including them as state variables in state estimation, which is addressed in Section 3.6.

3.3. Control Lyapunov function-based controller

A function V is a discrete-time exponentially stabilizing CLF (see Agrawal & Sreenath, 2017) for the system in Eq. (5), if there exists positive constants c_1, c_2, c_3 and a control input $u(t)$ (with $\underline{u} \le u(t) \le \bar{u}$) for all $x(t)$ (with $0 \le x(t) \le \bar{x}$) such that

$$c_1 \|x(t) - x_s\|^2 \le V(x(t) - x_s) \le c_2 \|x(t) - x_s\|^2 \tag{6}$$

$$V(x(t+1) - x_s) - V(x(t) - x_s) + c_3 \|x(t) - x_s\|^2 \le 0. \tag{7}$$

A straightforward choice for a Lyapunov function satisfying Eq. (6) is $V(x(t) - x_s) = \|x(t) - x_s\|^2$. A CLF-based controller (CLF-C) that renders (x_s, u_s) exponentially stable for the system (5) by explicitly enforcing Eq. (7) can be designed in the form of the following constrained optimization problem (based on the method of Agrawal & Sreenath, 2017) with a regulation objective:

$$\text{minimize}_u \quad \|x_+ - x_s\|^2_{Q_l} + \|u - u_s\|^2_{R_l} \tag{8}$$

$$\text{subject to} \quad V(x_+) - V(\tilde{x}(t)) \le -c_3 \|x\|^2 \tag{9}$$

$$x_+ = F(\tilde{x}(t), d_s, u) \tag{10}$$

$$\underline{u} \le u \le \bar{u}, \tag{11}$$

where x_+ is the one-step ahead predicted state, $Q_l \in \mathbb{R}^{n_x \times n_x}$ and $R_l \in \mathbb{R}^{n_u \times n_u}$ are positive-definite, symmetric weighting matrices expressing the regulation objective, $\tilde{x}(t)$ is the information about the state $x(t)$ (either measured or estimated) available at time step t, while c_3 is a positive constant, which can be tuned for ensuring a desired decay rate for the Lyapunov function (see §II.C in Galloway et al., 2015). Although not considered in this paper, design of Lyapunov functions is possible via, e.g., convex optimization-based methods considering objectives related to maximizing the decay rate or the domain of attraction size (see Johansen, 2000). Furthermore, it is also possible to consider improving control performance by using more sophisticated CLF-C formulations, for example by considering interpolation among several controllers (see, e.g., Rubin et al., 2020). Investigating improved CLF-C formulations for perimeter control via better design of the Lyapunov function and control algorithms can be an interesting direction for future research.

Using the CLF-C formulation it is possible to design feedback perimeter controllers addressing the tasks of stabilization and regulation. The problem (8) is a nonconvex nonlinear optimization problem of relatively small size, yielding a computationally efficient formulation. It can find potential use in situations where MPC might be unusable due to prohibitive computational burden (e.g., for MFDs systems with many regions; see computational efficiency results in Sirmatel & Geroliminis, 2018). Owing to lack of predictions, however, the CLF-C is restricted to myopic decisions and thus should not be expected to outperform MPC in terms of control performance.

3.4. Regulatory model predictive control

We consider here an MPC formulation addressing the regulation problem in feedback perimeter control, which involves steering the system state to a desired equilibrium (x_s, u_s). From the traffic engineering point of view, this corresponds to steering the accumulation of the urban network from an arbitrary (possibly highly congested) initial state to the equilibrium. The regulation problem can be cast as a nonlinear MPC formulation as follows:

$$\underset{\{u_k\}_{k=0}^{N_p-1}}{\text{minimize}} \quad \sum_{k=0}^{N_p-1} \|x_k - x_s\|^2_{Q_r} + \|u_k - u_s\|^2_{R_r} \tag{12}$$

$$\text{subject to} \quad x_0 = \tilde{x}(t) \tag{13}$$

$$\text{for } k = 0, \dots, N_p - 1: \tag{14}$$

$$x_{k+1} = F(x_k, d_s, u_k) \tag{15}$$

$$\underline{u} \le u \le \bar{u}, \tag{16}$$

where $k \in \mathbb{N}_0$ is the time interval counter, N_p is the prediction horizon, while $Q_r \in \mathbb{R}^{n_x \times n_x}$ and $R_r \in \mathbb{R}^{n_u \times n_u}$ are symmetric positive-definite weighting matrices defining the regulation stage cost expressing quadratic penalty on deviations from the equilibrium.

As is well-known in control literature (see Bitmead et al., 1990), closed-loop stability is not guaranteed using the MPC scheme Eq. (12). One of the standard approaches for establishing stability of the closed-loop under nonlinear regulatory MPC is the quasi-infinite horizon nonlinear MPC method proposed in Chen and Allgöwer (1998). This method involves adding a suitable terminal cost and a terminal state constraint to the regulatory nonlinear MPC problem (12), yielding the following formulation addressing the stabilization and regulation tasks:

$$\underset{\{u_k\}_{k=0}^{N_p-1}}{\text{minimize}} \quad \sum_{k=0}^{N_p-1} \|x_k - x_s\|_{Q_r}^2 + \|u_k - u_s\|_{R_r}^2 + \|x_{N_p} - x_s\|_{P_r}^2 \tag{17}$$

$$\text{subject to} \quad x_0 = \tilde{x}(t) \tag{18}$$

$$\text{for } k = 0, \dots, N_p - 1 : \tag{19}$$

$$x_{k+1} = F(x_k, d_s, u_k) \tag{20}$$

$$\underline{u} \le u \le \bar{u} \tag{21}$$

$$x_{N_p} \in \Omega_r, \tag{22}$$

where $P_r \in \mathbb{R}^{n_x \times n_x}$ is a symmetric positive-definite weighting matrix defining the terminal cost, whereas Ω_r is the terminal constraint set defined as (Chen & Allgöwer, 1998):

$$\Omega_r = \{x \in \mathbb{R}^{n_x} | x^T P_r x \le \alpha_r\}, \tag{23}$$

with α_r a positive constant.

Suppose that P_r and α_r are chosen such that Chen and Allgöwer (1998): (a) The terminal region Ω_r is control invariant for the system under a fictitious local linear feedback $u = u_s + K(x - x_s)$ (i.e., once the state x is inside Ω_r, it will stay inside, with the control input constraints satisfied for the local feedback, forever), (b) the terminal cost $\|x - x_s\|_{P_r}^2$ provides an upper bound for the infinite horizon cost (incurred for the original stage cost $\|x(t) - x_s\|_{Q_r}^2 + \|u(t) - u_s\|_{R_r}^2$) under the local feedback. Provided that the formulation and the dynamics satisfy some further assumptions (such as the dynamics being twice continuously differentiable), and if the problem is feasible at the first time step (i.e., at $t = 0$), then the system under closed-loop with the MPC (17) is asymptotically stable with a domain of attraction containing all initial states for which (17) is feasible (see Chen & Allgöwer, 1998 for a full discussion and the stability proof). The terminal ingredients P_r and α_r are to be chosen to satisfy the control invariance property, and there are several methods in the literature to compute them (see Chen et al., 2003 for a method considering ellipsoidal terminal regions based on solving a series of semidefinite optimization problems, and Cannon et al., 2003 for a method considering polytopic terminal regions). In particular, the method of Chen et al. (2003) (which is also used here) considers constructing a convex semidefinite optimization problem which involves simultaneously searching over the gain of a linear controller and an ellipsoidal set Ω_r, with the objective of maximizing the volume of Ω_r. The set is constructed to be control invariant under the linear controller, and inside the set the linear controller is stabilizing for the nonlinear system while satisfying state and input constraints.

Note that the quasi-infinite horizon NMPC method of Chen and Allgöwer (1998) is proposed for continuous-time nonlinear systems, however the example provided also in Chen and Allgöwer (1998) is implemented by taking a discrete-time formulation without any special modification of the method. We take the same approach in this paper to facilitate straightforward use of the method in practical implementation.

Using the quasi-infinite horizon regulatory MPC formulation (RMPC) it is possible to design feedback perimeter controllers addressing the tasks of stabilization and regulation. In addition to the recursive feasibility and closed-loop stability properties ensured by its construction, this formulation has the following important advantages (Chen & Allgöwer, 1998): (i) It yields the largest domain of attraction possible for a given terminal region Ω_r, as it ensures closed-loop stability for all initial states for which a system trajectory beginning at the initial state and terminating inside the terminal region Ω_r exists (i.e., for which the problem (17) is feasible). (ii) Globally optimal solutions are not required for achieving closed-loop stability; only feasible solutions are required. This is important because due to the nonlinear dynamics (5) the problem (17) is nonconvex and thus it is generally not possible to solve it to global optimality in real-time.

3.5. Economic model predictive control

We consider here an MPC formulation addressing the economic optimization problem for feedback perimeter control. Viewed together with the stabilization task, the economic optimization problem involves steering the system state from an initial state to the desired equilibrium while trying to approximate an economically optimal closed-loop system trajectory. From the traffic engineering point of view, the economic optimization problem corresponds to steering the accumulation of the urban network from an arbitrary (possibly highly congested) initial state to the equilibrium while attempting to achieve closed-loop accumulation trajectories that correspond to minimal TTS.

The economic optimization problem, corresponding to minimizing TTS for large-scale urban networks, can be cast as a nonlinear MPC problem as follows:

$$\underset{\{u_k\}_{k=0}^{N_p-1}}{\text{minimize}} \quad \sum_{k=0}^{N_p-1} \mathbf{1}^T x_k \tag{24}$$

$$\text{subject to} \quad x_0 = \tilde{x}(t) \tag{25}$$

$$\text{for } k = 0, \dots, N_p - 1 : \tag{26}$$

$$x_{k+1} = F(x_k, d_s, u_k) \tag{27}$$

$$\underline{u} \le u \le \bar{u}. \tag{28}$$

Similar to the case with regulatory MPC, the economic MPC formulation in Eq. (24) does not guarantee closed-loop stability. Closed-loop under economic nonlinear MPC can be established using the economic MPC formulation involving terminal cost and constraints proposed in Amrit et al. (2011). This method involves adding a suitable terminal cost and a terminal state constraint to the economic nonlinear MPC problem (24), yielding the following formulation addressing the stabilization and economic optimization tasks:

$$\underset{\{u_k\}_{k=0}^{N_p-1}}{\text{minimize}} \quad \sum_{k=0}^{N_p-1} \mathbf{1}^T x_k + \|x_{N_p} - x_s\|_{P_e}^2 \tag{29}$$

$$\text{subject to} \quad x_0 = \tilde{x}(t) \tag{30}$$

$$\text{for } k = 0, \dots, N_p - 1 : \tag{31}$$

$$x_{k+1} = F(x_k, d_s, u_k) \tag{32}$$

$$\underline{u} \le u \le \bar{u} \tag{33}$$

$$x_{N_p} \in \Omega_e, \tag{34}$$

where $P_e \in \mathbb{R}^{n_x \times n_x}$ is a symmetric positive-definite weighting matrix defining the terminal cost and Ω_e is the terminal constraint set defined as (Amrit et al., 2011):

$$\Omega_e = \{x \in \mathbb{R}^{n_x} | x^T P_e x \le \alpha_e\}, \tag{35}$$

with α_e a positive constant. Similar to the case with the stabilizing regulatory MPC (17), provided that P_e and α_e are chosen in such a way that Ω_e has n control invariance property, asymptotic stability of the closed-loop system are ensured by construction of the optimization problem (29) if it has a feasible solution at the first time step (i.e., at $t = 0$) (see Amrit et al., 2011 for a full discussion, stability proof, and a method to choose the terminal ingredients P_e and α_e).

3.6. Integrated state estimation and control

Presence of substantial measurement noise in practice might adversely affect control performance, necessitating the use of state estimators. Presence of additive process and measurement noise can be modeled by writing the dynamics (5) and measurement as:

$$x(t+1) = F(x(t), d(t), u(t)) + w(t) \tag{36}$$

$$y(t) = x(t) + v(t) \tag{37}$$

where $w \in \mathbb{R}^{n_x}$ is the process noise expressing uncertainty in the dynamics (with $w \sim \mathcal{N}(0, \Sigma_w)$), $y \in \mathbb{R}^{n_x}$ is the vector of measurements on x, whereas $v \in \mathbb{R}^{n_x}$ is the measurement noise vector (with $v \sim \mathcal{N}(0, \Sigma_v)$. A nonlinear state estimator can then be constructed in the form of the following MHE problem (based on Sirmatel & Geroliminis, 2019):

$$\underset{w_k}{\text{minimize}} \quad \sum_{k=-N_e}^{-1} \|w_k\|^2_{\Sigma_w^{-1}} + \sum_{k=-N_e}^{0} \|v_k\|^2_{\Sigma_v^{-1}} \tag{38}$$

$$\text{subject to} \quad \text{for } k = -N_e, \dots, 0: \tag{39}$$

$$v_k = y(t+k) - x_k \tag{40}$$

$$x_k \in \mathcal{X} \tag{41}$$

$$\text{for } k = -N_e, \dots, -1: \tag{42}$$

$$x_{k+1} = F(x_k, d_s, u(t+k)) + w_k \tag{43}$$

where N_e is estimation horizon, t is the current time step, Σ_w and Σ_v are covariance matrices of the process and measurement noise, respectively, whereas the set $\mathcal{X}$ denotes known physical constraints on the state such as accumulations being non-negative. A detailed study on MFD-based MHE formulations considering incomplete measurements and inflow demand estimation can be found in Sirmatel and Geroliminis (2019).

In practice, the inflow demands $d(t)$ can be unknown and time-varying, and it might be impossible to measure them due to lack of appropriate sensors or privacy issues. However, the perimeter control methods discussed in this paper necessitate having information on the demands, as it is required both for the prediction models and for calculating the equilibrium state x_s. Even if the demands are unknown, they can be estimated via including them in state estimation as constant but unknown state variables, leading to the following augmented dynamical model (following the approach in Sirmatel & Geroliminis, 2019):

$$x(t+1) = F(x(t), d(t), u(t)) + w(t) \tag{44}$$

$$d(t+1) = d(t) + w_d(t) \tag{45}$$

where $w_d \in \mathbb{R}^{n_x}$ is a process noise term representing the uncertainty in modeling the inflow demands as constant. Although potentially inaccurate when the inflow demands have strong sustained fluctuations in time, such an approach is shown in Sirmatel and Geroliminis (2019) to be reasonably well performing for the cases where complete or partial measurements (i.e., $q_i = \sum_{j \in \mathcal{R}} q_{ij}$ are measured) are available on the inflow demands.

A traffic management scheme integrating state estimation and control can be designed using the estimator given in Eq. (38) together with one of the controllers presented in Eqs. (8), (17) and (29). Operation of the scheme is formalized in Algorithm 1.

The problems in Eqs. (8), (12) and (24) are nonconvex nonlinear optimization problems, which can be solved reliably and efficiently via, e.g., sequential quadratic programming or interior point solvers (for details, see Diehl et al., 2009). Using the dynamics (2) for a network with a reasonable size, the problem (17) is real time tractable (i.e., the CPU time needed to solve one instance of the problem is around a couple of seconds and thus negligible compared to the usual sampling time values of around 90 seconds that are chosen equal to the length of the traffic light cycle; see computational efficiency results in §III.B of Sirmatel & Geroliminis, 2018 for a network with 7 regions). For MFD networks with many regions, the formulations might lose computational tractability. Another challenge (even if computational efficiency could be improved through stronger software and/or hardware) is that a large number of regions will require a more careful treatment of route choice which will require a dynamical model with higher complexity, causing difficulties in both control/estimator design (due to increased state and input dimensions and model complexity) and instrumentation (due to increased number and sophistication of required sensors and actuators).

Algorithm 1 Operation of state estimation and control.

Initialize simulation from $x(0)$ at $t = 0$. Then, at each time step t:

(1) Given measurements $\{y(t+k)\}_{k=-N_e}^{0}$ and control inputs $\{u(t+k)\}_{k=-N_e}^{-1}$, solve the MHE problem (38) to obtain the state estimate $\hat{x}(t)$.

(2) Using the state estimate as available information, i.e., $\tilde{x}(t) = \hat{x}(t)$, solve the optimization problem (either one of Eqs. (8), (17) and (29)) to obtain control input $u(t)$.

(3) Apply the control input $u(t)$ to the plant; if simulating, evolve system dynamics given in Eq. (5).

Repeat steps 1, 2, and 3 for $t \in \mathbb{Z}_{\geq 0}$ up to t_{final}.

4. Results

In this section we examine the performance and domain of attraction properties of the controllers presented in Section 3 by computer simulations. We construct scenarios where the concern is to recover the city traffic from highly congested conditions and steer it back to operating at equilibrium. Detailed analyses are provided for two individual congested scenarios for both macroscopic and microscopic simulation (considering a single initial state for each). Extensive macroscopic simulations are used to construct domains of attraction (by creating a grid on the regional accumulation space and using each grid point as the initial state for a simulation experiment), for cases of control under no uncertainty, control under uncertainty, and control under uncertainty with joint state estimation.

4.1. Network description and simulation setup

We consider a two-region MFDs network for macroscopic simulations (see Fig. 1(a)), where the *plant* representing reality is a macroscopic simulator built via Eq. (5). The peripheral region (region 1) having jam accumulation of $n_1^{\text{jam}} = 26800$ veh, a critical accumulation of $n_1^{\text{cr}} = 8933$ veh, and a capacity flow of $g_1(n_1^{\text{cr}}) = 20.15$ veh/s, while the central region (region 2) has a jam accumulation of $n_2^{\text{jam}} = 22000$ veh, a critical accumulation of $n_2^{\text{cr}} = 7333$ veh, and a capacity flow of $g_2(n_2^{\text{cr}}) = 14.4$ veh/s. The perimeter control input constraints are $u_{\min} = 0.1$ and $u_{\max} = 0.9$. To yield an equilibrium point, we can chose first the inflow demands as $q_{11,s} = 6$ veh/s, $q_{12,s} = 5$ veh/s, $q_{21,s} = 4$ veh/s, $q_{22,s} = 2$ veh/s, which represent moderate feasible demand, and the perimeter control inputs at the equilibrium are chosen as $u_{12,s} = 0.60$ and $u_{12,s} = 0.62$, which represent usual values in uncongested operation. From $x_s = F(x_s, d_s, u_s)$, we obtain the accumulation states at the equilibrium as $n_{11,s} = 3232$ veh, $n_{12,s} = 2649$ veh, $n_{21,s} = 2581$ veh, $n_{22,s} = 2763$ veh, corresponding to equilibrium regional accumulations $n_{1,s} = 5881$ veh and $n_{2,s} = 5344$ veh. For the microscopic simulations, MFD parameters (i.e., a_i, b_i, and c_i in Eq. (1)) required for the prediction model are found by fitting third degree polynomial to accumulation versus outflow data taken from a microscopic simulation experiment with no control. Sampling time is chosen as $T = 90$ s to reflect a realistic value of traffic light cycle duration. Terminal costs and constraints required for the stabilizing MPC formulations Eqs. (12)

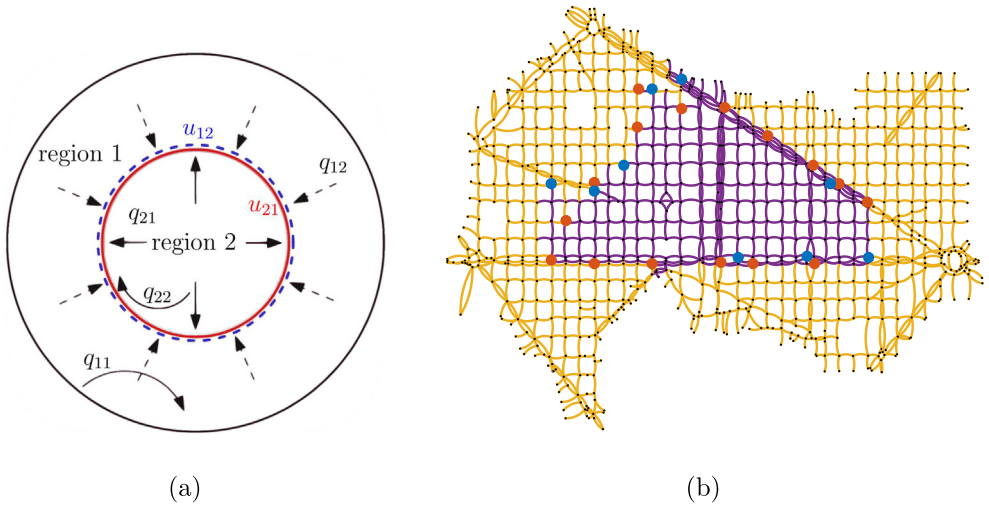

Fig. 1. (a) Schematic representation of a two region network. (b) Microscopic simulation (Aimsun) model of a real traffic network, with clustering results as links (region 1 in yellow and region 2 in purple) and controlled intersections as disks (intersections belonging to u_{12} in blue and u_{21} in red). (For interpretation of the references to color in this figure legend, the reader is referred to the web version of this article.)

and (24) are computed considering the problem data and using the methods proposed in Chen et al. (2003) and Amrit et al. (2011), for the regulatory and economic NMPC formulations, respectively. The parameter c_3, specifying the decay rate for the CLF-C, is chosen as 10^{-8} to choose a value that yields a large domain of attraction. Additional simulation studies (which we omit for brevity) revealed that the results do not change significantly when c_3 varies within the range $10^{-8} \leq c_3 \leq 10^{-2}$; there are no substantial changes in either the domain of attraction or regulation performance within this range. Increasing c_3 beyond 10^{-2} results in noticeable decrease in the domain of attraction size, with virtually no improvement in regulation performance. Further research on CLF-based perimeter control schemes is needed to examine these in detail.

Due to being computationally lightweight (with a single no control simulation experiment taking less than a second), macroscopic simulations are essential for being able to conduct large numbers of repetitions such as those required for numerically constructing the domains of attraction. Nevertheless, evaluating traffic control algorithms for achieving reasonable trust in their practical performance requires the use of microscopic simulations. While macroscopic simulations simply make use of numerical integration employing the dynamical equations (such as those given in Eq. (2)), microscopic simulations involve sophisticated traffic simulation software that can simulate the behavior of individual vehicles with human drivers. Such simulations are capable of generating results of traffic scenarios with tens of thousands of vehicles interacting with each other and an urban road traffic network taken from a real city. An important downside to microscopic simulations is their excessive computational burden, with a single simulation experiment requiring hours to finish execution.

For microscopic simulations we also consider a two region urban road traffic network (see 1), where the *plant* representing reality is a model replicating a real traffic network having around 1500 links and 600 intersections using the microscopic simulation package Aimsun. The model represents a portion of the urban network of the city of Barcelona in Spain, with an area of 12 km^2, which is partitioned into two regions using the optimization-based clustering method of Saeedmanesh and Geroliminis (2016). The simulations involve vehicles that adapt to traffic conditions and dynamically update their routes using real-time traffic information and a predefined dynamic traffic assignment strategy. Only a subset of the traffic signals (25 out of 600; see the disks in 1) at the boundary of the two regions are used as actuators of the developed controllers (as per the perimeter control approach), while the remaining operate with pre-timed signals. Control inputs are implemented by changing the ratio of durations of green and red lights accordingly for the corresponding intersections. For example, if a control input value of $u_{12}(t) = 0.7$ is computed, the green and red light durations are set to 63 and 27 s for the 90 s period between time steps t and $t+1$, respectively, for the intersections belonging to the perimeter control input u_{12} (i.e., the blue disks in 1). Actual fixed-time plans of the city (as captured by the microscopic simulation model) are applied to the rest of the intersections, i.e., those that are not connected to the control inputs (for more details see Kouvelas et al., 2017a).

For ensuring that the economic stage cost $\mathbf{1}^T x_k$ (expressing TTS) conforms to the requirements of the economic MPC formulation with guaranteed closed-loop stability as proposed in Amrit et al. (2011), it is slightly modified as follows:

$$l(x_k, u_k) = \mathbf{1}^T x_k + l_e(x_k, u_k), \tag{46}$$

where $l_e(\cdot)$ is a regularization term that is needed to ensure strict dissipativity of the system for the supply rate $l(x,u) - l(x_s,u_s)$ (which is required for closed-loop stability under the MPC (29); see definition 1 and assumption 4 in Amrit et al., 2011), which is chosen in the following form:

$$l_e(x_k, u_k) = \|x_k - x_e\|^2_{Q_e} + \|u_k - u_e\|^2_{R_e}, \tag{47}$$

where $Q_e \in \mathbb{R}^{n_x \times n_x}$, $R_e \in \mathbb{R}^{n_u \times n_u}$, and $P_e \in \mathbb{R}^{n_x \times n_x}$ are symmetric positive-definite weighting matrices expressing a quadratic penalty on the deviations from the regularization point (x_e, u_e). The numerical values for the regularization term are chosen as $Q_e = 0.1 \cdot I$, $R_e = 100 \cdot I$, $x_e = 3000 \cdot \mathbf{1}$ veh, and $u_e = 0.6 \cdot \mathbf{1}$, which are chosen large enough by trial-and-error to ensure strict dissipativity.

4.2. Congested scenario via macroscopic simulation

Here we examine a single traffic scenario, where the peripheral region is initially highly congested, with the system having an initial state of $n_{11}(0) = 8000$ veh, $n_{12}(0) = 8000$ veh, $n_{21}(0) = 0$ veh, $n_{22}(0) = 0$ veh. Results of four macroscopic simulation experiments showing trajectories of accumulation state n_{ij}, perimeter control input u_{ih}, regional accumulations on n_1-n_2 space, and total exit flow $\sum_{i \in \mathcal{R}} m_{ii}(t)$, comparing the CLF-C, stabilizing regulatory NMPC (RMPC), stabilizing economic NMPC (EMPC), and purely economic NMPC (pure EMPC, i.e., Eq. (24)), with the MPCs having a prediction horizon of $N_p = 40$, are given in Fig. 2, for a time period corresponding to about 4 hours of real time.

From the figure it can be seen that all controllers are successful in steering the system state to an equilibrium, with the MPC controllers

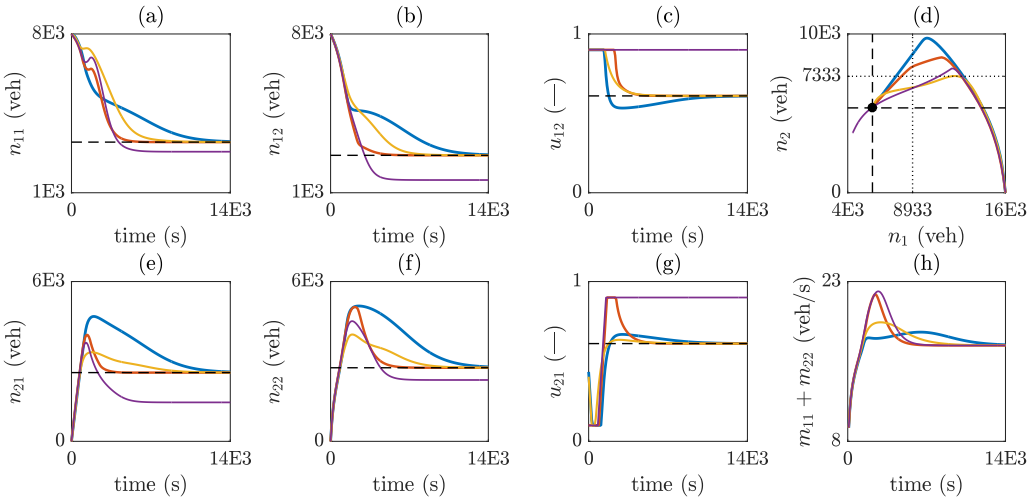

Fig. 2. Accumulation state n_{ij}, perimeter control input u_{ih}, and total exit flow $\sum_{i\in\mathcal{R}} m_{ii}(t)$ trajectories for a congested scenario obtained via macroscopic simulation, comparing CLF-based controller (blue), regulatory NMPC (red), economic NMPC (yellow), and purely economic NMPC (purple): (a) $n_{11}(t)$, (b) $n_{12}(t)$, (c) $u_{12}(t)$, (d) $n_1(t)$-$n_2(t)$, (e) $n_{21}(t)$, (f) $n_{22}(t)$, (g) $u_{21}(t)$, (h) $m_{11}(t) + m_{22}(t)$. Dashed lines show equilibrium values, while for (d) dotted lines show the critical accumulations n_i^{cr}. (For interpretation of the references to color in this figure legend, the reader is referred to the web version of this article.)

having a substantially better performance. For all three stabilizing controllers, stability is guaranteed by construction, as the controller formulations result in stabilizing closed-loop control if they are feasible for the initial state, which is confirmed here in simulation. The importance of this from the traffic point of view is that stability is essential in ensuring reliable and efficient operation of traffic control systems and achieving high mobility in urban networks.

Note that the RMPC being able to bring the system to equilibrium faster than EMPC is related to the fact that EMPC uses the modified stage cost Eq. (46) instead of the purely economic one $\mathbf{1}^T x_k$. This modification is required for using the economic MPC formulation of Amrit et al. (2011) with guaranteed closed-loop stability; pure EMPC cannot be used with the method of Amrit et al. (2011) as the purely economic stage cost $\mathbf{1}^T x_k$ does not yield strict dissipativity. Regulation performance of the pure EMPC is comparable to that of the stabilizing RMPC, both of which are superior to that of the stabilizing EMPC. This suggests that exploring stability of other MPC formulations permitting use of purely economic costs is an interesting direction for future research, as it can potentially yield high performance stabilizing EMPC methods for feedback perimeter control. Note also that these results are for the nominal case where there is no modeling and measurement uncertainty, and for progress towards more practical feedback perimeter control schemes, robust control formulations should be studied where uncertainty is considered in the control problem formulation (see Haddad, 2015 for a study considering robust perimeter control design using a linear model). Note also that the pure EMPC converges to a different equilibrium, which is related to the fact that the equilibrium x_s is not unique for fixed inflow demand d_s, since it also depends on u_s, and the pure EMPC, not being restricted to converging to u_s due to its purely economic objective, causes the closed-loop system to converge to a different equilibrium.

4.3. Congested scenario via microscopic simulation with time-varying unknown demands

The case of time-varying unknown inflow demands can be addressed by including them in state estimation as in Eq. (44), modeling them as additional state variables to be estimated. We examine here a single macroscopic simulation scenario, with the system having an initial state of $n_{11}(0) = 6000$ veh, $n_{12}(0) = 6000$ veh, $n_{21}(0) = 4000$ veh, $n_{22}(0) = 4000$ veh, for three different cases of measurements available on the inflow demands: (a) No measurements available, (b) regional inflow demands (i.e., $q_i(t)$, for $i \in \mathcal{R}$, with $q_i(t) = \sum_{j\in\mathcal{R}} q_i j(t)$) are measured, (c) all inflow demands (i.e., $q_i j(t)$, for $i, j \in \mathcal{R}$) are measured. The scenario involves a stabilizing regulatory MPC coupled with an MHE using the model Eq. (44), and is otherwise the same as the one presented in the previous section with the congested scenario using macroscopic simulation. The overall procedure however is the same for other types of controllers, as it relies on using a state estimator to estimate the inflow demands and use the estimated values when evaluating the prediction model of the controller, and calculating the equilibrium state in real-time as a function of the inflow demands (provided that the demands are feasible, i.e., an equilibrium state exists for the demands) and modifying the setpoints of the controllers accordingly. Results of three macroscopic simulation experiments showing trajectories of accumulation state n_{ij}, perimeter control input u_{ih}, regional accumulations on n_1-n_2 space, total exit flow $\sum_{i\in\mathcal{R}} m_{ii}(t)$, together with true and estimated inflow demands q_{ij}, comparing the cases with no measurements, partial measurements, and full measurements on q_{ij}, with the MPC having a prediction horizon of $N_{\mathrm{p}} = 40$, are given in Fig. 3, for a time period corresponding to about 9 hours of real time.

From the figure we can make the following observations: In the practically relevant case of unknown and time-varying demands, even when no measurements on inflow demands are available, it is possible to estimate them using a state estimator, and to successfully conduct congestion recovery control using stabilizing MPC. Furthermore, as expected, higher information content in the q_{ij} measurements leads to better estimation performance. Although it is omitted here for brevity, the cases where inflow demands have continuously varying profiles can also be handled in the same way (see Sirmatel & Geroliminis, 2019).

4.4. Congested scenario via microscopic simulation

Here we examine a single microscopic simulation experiment, where a scenario involving an initially highly congested network (with $n_{11}(0) = 5166$ veh, $n_{12}(0) = 6822$ veh, $n_{21}(0) = 7457$ veh, $n_{22}(0) = 5114$ veh) together with a feasible constant demand is considered. The controllers are designed and tuned in the same manner as those considered in Section 4.2 with the following extensions: (1) Sensor noise is added to the accumulation state measurements as $y_{ij}(t) = n_{ij}(t) + v_{ij}(t)$, with $v_{ij}(t) \in \mathcal{N}(0, \sigma_v)$ and $\sigma_v = 250$ veh corresponding to a moderate amount of noise, to reflect a practice-oriented scenario where measurements are corrupted by noise, (2) controllers are deployed together with a MHE scheme having an estimation horizon of $N_{\mathrm{e}} = 20$ to mitigate the adverse effects of measurement noise, (3) MFD parameters are obtained via fitting third degree polynomials to data from a no-control microscopic

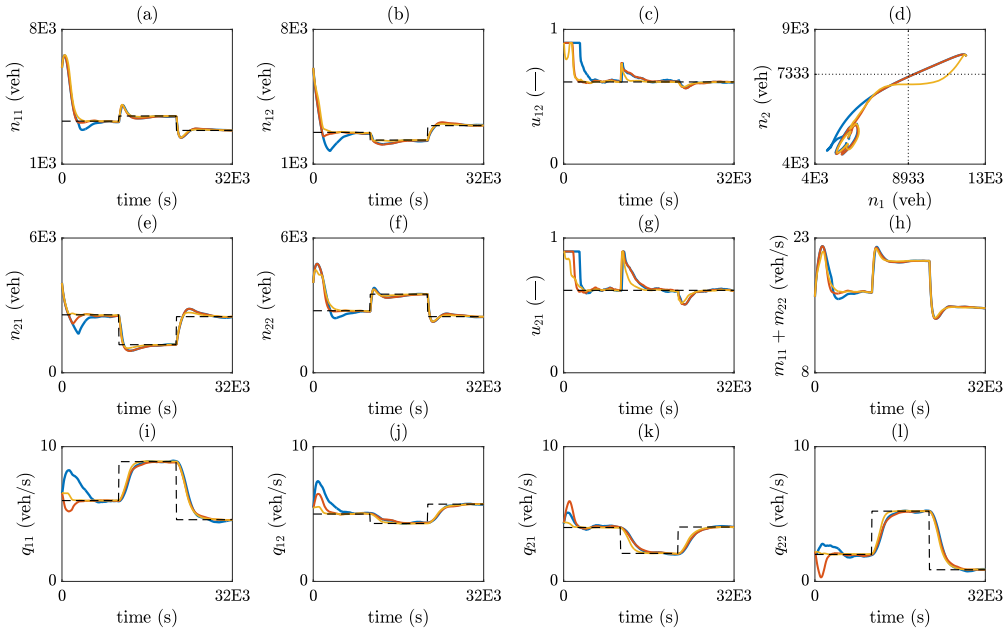

Fig. 3. Accumulation state n_{ij}, perimeter control input u_{ih}, total exit flow $\sum_{i\in\mathcal{R}} m_{ii}(t)$, together with true (dashed lines) and estimated (solid lines) inflow demand q_{ij} trajectories, for a congested scenario obtained via macroscopic simulation using regulatory NMPC with MHE considering q_{ij} estimation, comparing the cases with no measurements on q_{ij} (blue), measurements on q_i (red), and measurements on q_i (yellow): (a) $n_{11}(t)$, (b) $n_{12}(t)$, (c) $u_{12}(t)$, (d) $n_1(t)$-$n_2(t)$, (e) $n_{21}(t)$, (f) $n_{22}(t)$, (g) $u_{21}(t)$, (h) $m_{11}(t) + m_{22}(t)$, (i) $q_{11}(t)$, (j) $q_{12}(t)$, (k) $q_{21}(t)$, (l) $q_{22}(t)$. Dashed lines show equilibrium values. (For interpretation of the references to color in this figure legend, the reader is referred to the web version of this article.)

simulation. Measurement noise is clipped to values within two standard deviations of the mean, so as to avoid potentially unrealistic extreme values. Results of four microscopic simulation experiments showing trajectories of accumulation state n_{ij}, perimeter control input u_{ih}, regional accumulations on n_1-n_2 space, and total exit flow $\sum_{i\in\mathcal{R}} m_{ii}(t)$, comparing the CLF-C, stabilizing regulatory NMPC (RMPC), stabilizing economic NMPC (EMPC), and purely economic NMPC (pure EMPC, i.e., Eq. (24)), with the MPCs having a prediction horizon of $N_p = 40$, are given in Fig. 4, for a time period corresponding to about 5.5 h of real time. The accumulation versus outflow data together with the functional forms (i.e., polynomials fitted to the data) of the outflow MFDs, for the four experiments with the different controllers (also showing those of a no control scenario used to extract the functional forms of the MFDs used in the dynamical models for control design), are shown in Fig. 5. Snapshots of the traffic network for the same four experiments, for the first 3.75 h, showing road link occupancies in percentages taken in steps of 45 min, are given in Fig. 6.

From Fig. 4 it can be seen that all controllers are capable of steering the system back to lightly congested conditions, indicating a successful congestion recovery operation, with the regulatory MPC having a better performance. The MFDs in Fig. 5 suggest that the scenario involves severe levels of congestion for both regions, with accumulations well above the critical accumulation as indicated by the accumulation versus outflow data points on the right half of the MFDs. From Fig. 6 performance of the controllers can be seen in link-level detail, where the initial high congestion spreads over the network and eventually dissipates, with varying rates of dissipation depending on controller performance, as the system returns to equilibrium. Moreover, Fig. 6 shows that congestion level of links in close proximity to the perimeter control actuated intersections (i.e., the red and blue disks) are similar to that of the rest of the network. This suggests that the effect of perimeter control actions on boundary queues are tolerable, since they do not cause any high level of congestion that is not already present in other parts of the network. These results suggest that deploying MPC together with MHE has a strong potential for practical high performance large-scale urban traffic control even in the presence of measurement noise.

For dynamical systems subject to control input constraints it may not be possible to guarantee stability for all possible initial states. In the next section we examine, via simulations, the domains of attraction for the closed-loop system under the three controllers.

4.5. Simulation-based construction of domains of attraction

4.5.1. Control under no uncertainty

To investigate the domain of attraction properties of the controllers for the two-region MFDs system, we present here a series of simulation experiments on a grid of initial accumulation state values $x(0)$. The simulations are conducted using the dynamical Eqs. (5) as simulator, with the process noise $w(t)$ and measurement noise $v(t)$ terms set to zero to reflect the no uncertainty situation. The set of initial states that are important for the traffic point of view for the two-region MFDs system is those that have a regional accumulation between 0 and jam accumulation, which correspond to $0 \le n_1(0) \le 26800$ veh and $0 \le n_2(0) \le 22000$ veh for the considered problem data. To be able to consider a two-dimensional domain of attraction for visualization purposes, the initial states of each simulation experiment is chosen to be extracted as half of the initial regional accumulation (e.g., for a scenario with $n_1(0) = 8000$ veh and $n_2(0) = 12000$, the initial state is $n(0) = [4000\ 4000\ 6000\ 6000]^T$ (veh)). Each grid point on the n_1-n_2 space of initial states, with increments of 1000 veh, up to the jam accumulation for each region, is simulated with the no control case (where $u(t) = u_s$) and the three controllers, using various prediction horizon values for the MPCs. The results are shown in Fig. 7, depicting boundaries of the domains of attraction and phase portraits (with all initial states and state trajectories projected from the four-dimensional state space onto two-dimensional n_1-n_2 space for visualization purposes).

The results in Fig. 7 suggest that it is possible to stabilize a substantial section of the n_1-n_2 space of initial states using the proposed MPCs, and that the domain of attraction can be enlarged by increasing the prediction horizon, as expected. Although not capable of reducing TTS as much as the MPCs (as shown in the previous section), owing largely to absence of predictions, the CLF-C still has a decent domain of attraction (comparable with the MPCs with $N_p = 30$).

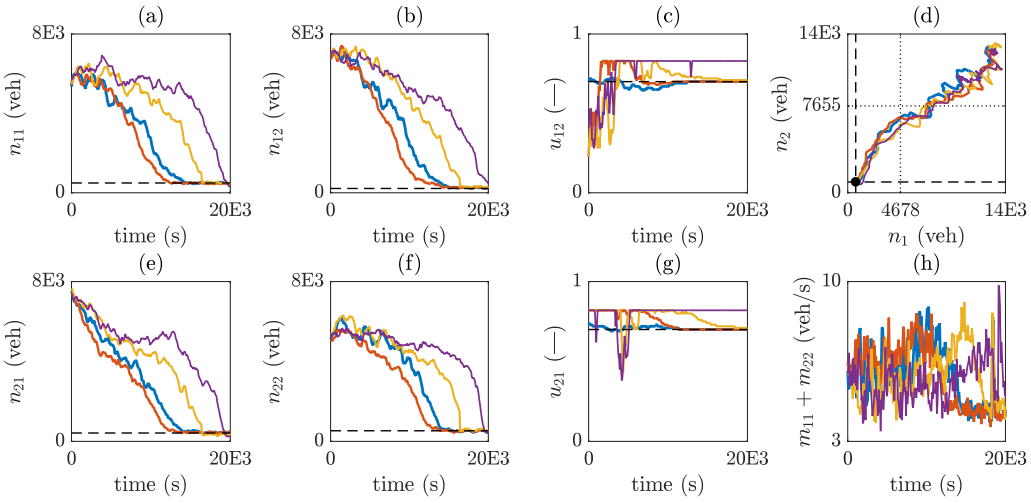

Fig. 4. Accumulation state n_{ij}, perimeter control input u_{ih}, and total exit flow $\sum_{i\in R} m_{ii}(t)$ trajectories for a congested scenario obtained via microscopic simulations, comparing CLF-based controller (blue), regulatory NMPC (red), economic NMPC (yellow), and purely economic NMPC (purple): (a) $n_{11}(t)$, (b) $n_{12}(t)$, (c) $u_{12}(t)$, (d) $n_1(t)$-$n_2(t)$, (e) $n_{21}(t)$, (f) $n_{22}(t)$, (g) $u_{21}(t)$, (h) $m_{11}(t) + m_{22}(t)$. Dashed lines show equilibrium values, while for (d) dotted lines show the critical accumulations n_i^{cr}. (For interpretation of the references to color in this figure legend, the reader is referred to the web version of this article.)

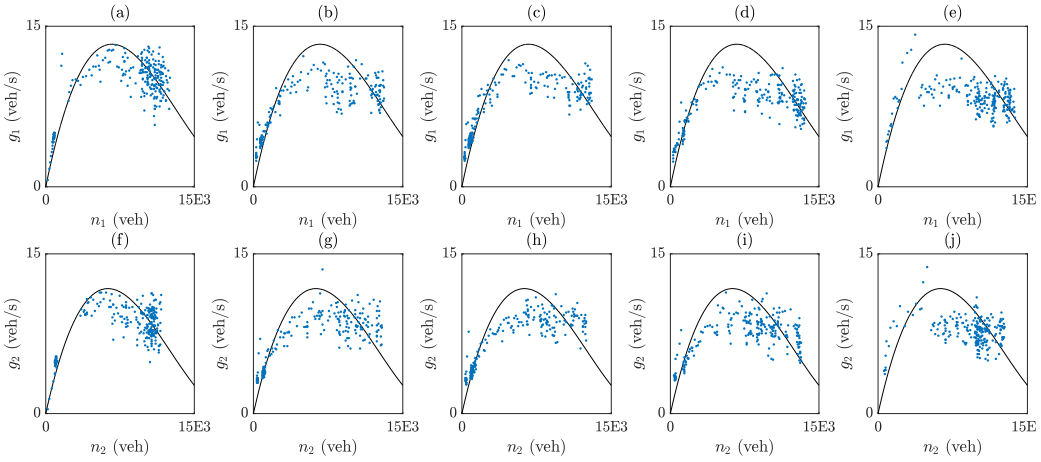

Fig. 5. Outflow MFDs, showing the functional forms $g_i(n_i)$ (black) together with accumulation versus outflow data (blue), from microscopic simulation, for region 1 (a)–(e) and region 2 (f)–(j), for the no control scenario conducted for obtaining the MFDs (a), (f), CLF-based controller (b), (g), regulatory NMPC (c), (h), economic NMPC (d), (i), and purely economic NMPC (e), (j). (For interpretation of the references to color in this figure legend, the reader is referred to the web version of this article.)

4.5.2. Control under uncertainty

Control performance and stabilization properties might be adversely affected in the presence of uncertainty in the model and measurement noise. Here we investigate the effect of these by using various levels of uncertainty in the simulations. The same set of simulations as in the previous section is conducted here, the only difference being the introduction of process noise $w(t)$ and measurement noise $v(t)$. Standard deviations of the process and measurement noise terms are chosen as $\sigma_w = \{0.5, 1, 1.5, 2\}$ veh/s and $\sigma_v = \{500, 1000, 1500, 2000\}$ veh, respectively, indicating a range of moderate to severe modeling and measurement uncertainty. Process and measurement noises are clipped to values within two standard deviations of the mean, so as to avoid potentially unrealistic extreme values. The controllers use the measured state $y(t)$ as available information $\tilde{x}(t)$. The results are shown in Fig. 8, depicting boundaries of the domains of attraction (with all initial states and state trajectories projected from the 4D n-space onto 2D n_1-n_2 space for visualization purposes).

From the results in Fig. 8 it can be seen that increasing the level of uncertainty decreases size of the domain of attraction, as expected. For low uncertainty values, the controllers are able to keep their domains of attractions roughly the same as those in the no uncertainty case, while for high uncertainty the domains of attractions suffer from decreases in size up to 30%. These results reveal that some of the highly congested traffic conditions cannot be recovered and brought back to equilibrium state using these controllers when operating under modeling and measurement uncertainty, indicating a severe loss of authority for the controllers. Using state estimation can alleviate some of the problems related to measurement noise, which is investigated in the following section.

4.5.3. Joint control and state estimation under uncertainty

Domain of attraction size lost due to uncertainty can be partially recovered using state estimation. Here we investigate the effect of using state estimation on the domain of attraction by using various levels of uncertainty in the simulations. The same set of simulations as in the previous section is conducted here, with the only difference being the controllers having access to state estimates computed by the nonlinear MHE (38) with an estimation horizon of $N_{\mathrm{e}} = 20$. The controllers thus use the state estimate $\hat{x}(t)$ as available information $\tilde{x}(t)$. The results are shown in Fig. 9, depicting boundaries of the domains of attraction (with all initial states and state trajectories projected from the 4D n-space onto 2D n_1-n_2 space for visualization purposes), and in Fig. 10, depicting a size comparison of the domains of attraction shown in Fig. 8

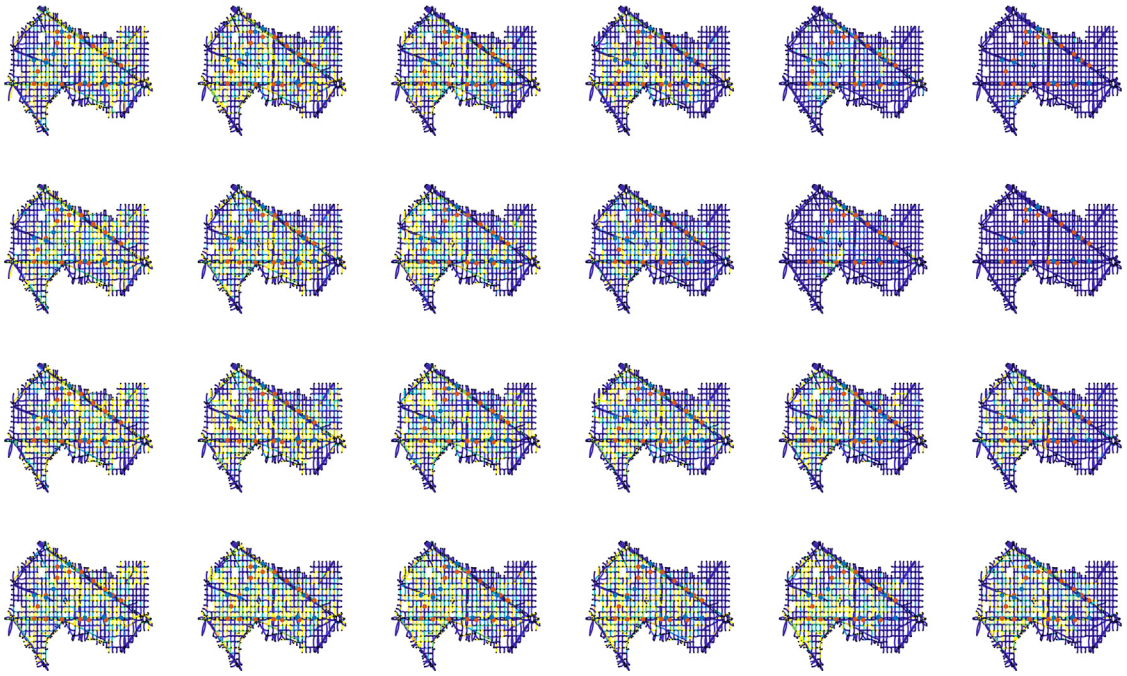

Fig. 6. Snapshots of link occupancies shown on the microscopic simulation model of the traffic network, for the first 3.75 hours of the microscopic simulation experiment in steps of 45 minutes (light yellow is 100%, dark blue is 0% occupancy) comparing CLF-C (first row), regulatory NMPC (second row), economic NMPC (third row), and purely economic NMPC (fourth row). Controlled intersections are shown as disks (intersections belonging to u_{12} in blue and u_{21} in red). (For interpretation of the references to color in this figure legend, the reader is referred to the web version of this article.)

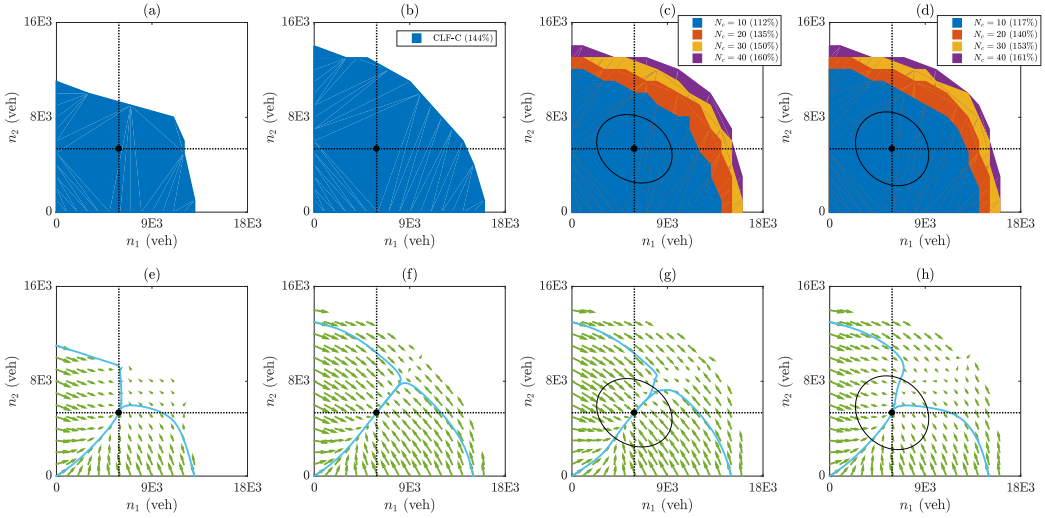

Fig. 7. Domains of attraction (a)–(d) and the phase portraits (for $N_p = 40$ for MPCs) (e)–(h) for the no control case (a),(e), the CLF-C (b),(f), the regulatory NMPC (c),(g), and the economic NMPC (d),(h) for the no uncertainty case. Three selected closed-loop state trajectories are shown on the phase portraits in light blue, equilibrium point is shown as a black dot, while the boundaries of the ellipsoidal terminal constraint sets are shown in black for the MPC controllers. Percentages denote the ratio of the domain size to that of the no control case. (For interpretation of the references to color in this figure legend, the reader is referred to the web version of this article.)

and Fig. 9, where the overall noise is summarized by a noise level γ, with $\sigma_w = \gamma \cdot 0.5$ veh/s and $\sigma_v = \gamma \cdot 500$ veh.

From the results in Fig. 9 it can be seen that using state estimation has a substantial effect in recovering domain of attraction, as the loss in size due to uncertainty in this case is up to 8%, as opposed to the values up to 30% for the case without state estimation. The results in Fig. 10 suggest that the CLF-C is not particularly sensitive to noise, while for MPC substantial parts of the domain of attraction can be lost due to uncertainty. However the figure also shows that using MHE it can be recovered to a great extent, as for joint MHE-MPC the domain of attraction appears to be largely insensitive to noise. These results suggest that using state estimation, especially for operation of MPC under high levels of uncertainty, is required to maintain control authority over larger domains of attraction in recovering from highly congested traffic situations.

5. Conclusion

In this paper we proposed application of nonlinear MPC formulations with guaranteed closed-loop stability, for the regulation and economic optimization problems, to feedback perimeter control design for MFDs networks. A discrete-time control Lyapunov function-based controller is also proposed to serve as a non-predictive benchmark. Performance in increasing mobility and domain of attraction properties of the proposed controllers are examined via macroscopic and

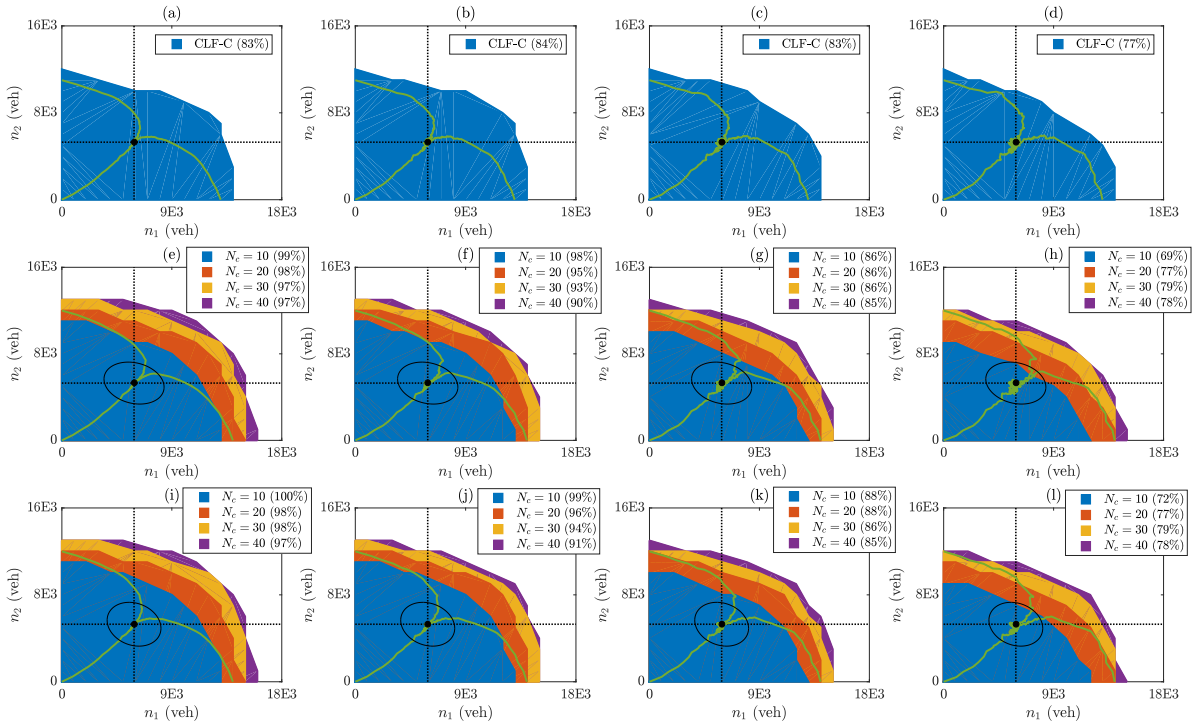

Fig. 8. Domains of attraction for the CLF-C (a)–(d), the regulatory NMPC (e)–(h), and the economic NMPC (i)–(l), for the uncertainty case: (a)–(e)-(i) $\sigma_w = 0.5$ veh/s and $\sigma_v = 500$ veh, (b)–(f)-(j) $\sigma_w = 1$ veh/s and $\sigma_v = 1000$ veh, (c)–(g)-(k) $\sigma_w = 1.5$ veh/s and $\sigma_v = 1500$ veh, (d)–(h)-(l) $\sigma_w = 2$ veh/s and $\sigma_v = 2000$ veh. Three selected closed-loop state trajectories (with $N_p = 30$ for MPCs) are shown in green, while the terminal constraint sets are shown in black for the MPC controllers. Percentages denote the ratio of the domain compared to its no uncertainty counterpart in terms of size. (For interpretation of the references to color in this figure legend, the reader is referred to the web version of this article.)

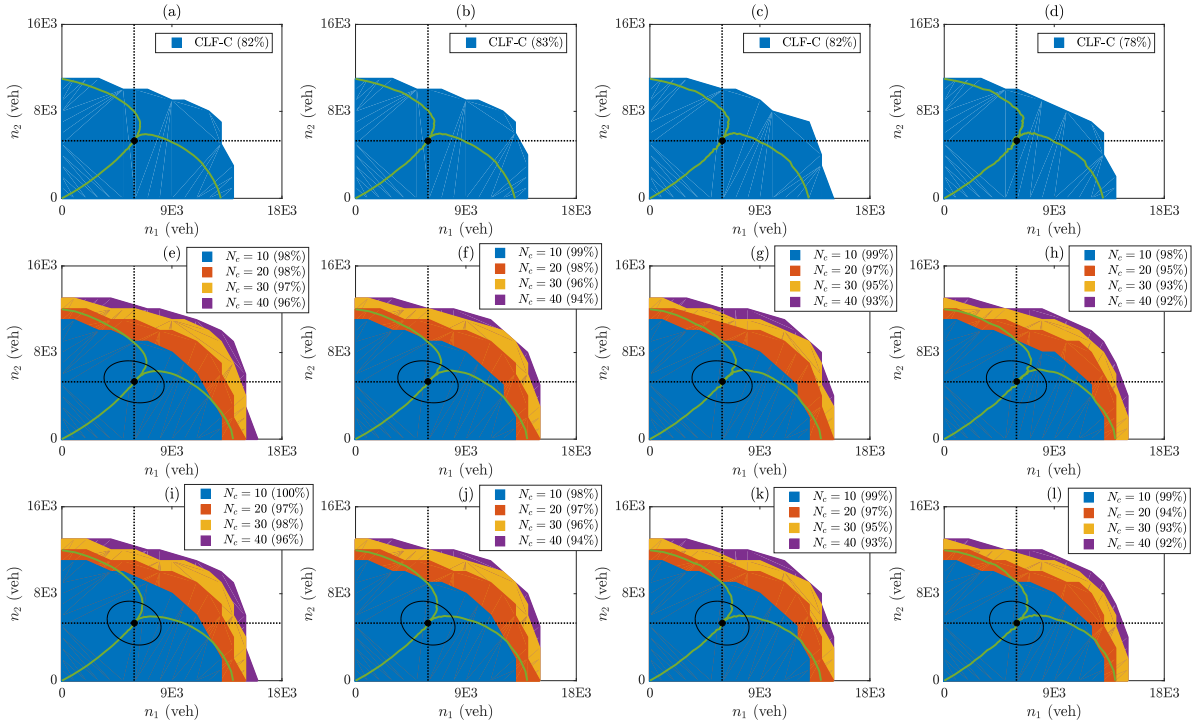

Fig. 9. Domains of attraction for the CLF-C (a)–(d), the regulatory NMPC (e)–(h), and the economic NMPC (i)–(l), for the uncertainty case with joint state estimation: (a)–(e)-(i) $\sigma_w = 0.5$ veh/s and $\sigma_v = 500$ veh, (b)–(f)-(j) $\sigma_w = 1$ veh/s and $\sigma_v = 1000$ veh, (c)–(g)-(k) $\sigma_w = 1.5$ veh/s and $\sigma_v = 1500$ veh, (d)–(h)-(l) $\sigma_w = 2$ veh/s and $\sigma_v = 2000$ veh. Three selected closed-loop state trajectories (with $N_p = 30$ for MPCs) are shown in green, while the terminal constraint sets are shown in black for the MPC controllers. Percentages denote the ratio of the domain compared to its no uncertainty counterpart in terms of size.

microscopic simulation experiments with and without modeling and measurement uncertainty. Properties of joint state estimation and control in dealing with measurement uncertainty are also investigated. Results indicate that through nonlinear MPC schemes with guaranteed stability it is possible to stabilize a substantial portion of the state space for perimeter controlled MFD networks. Although increasing level of

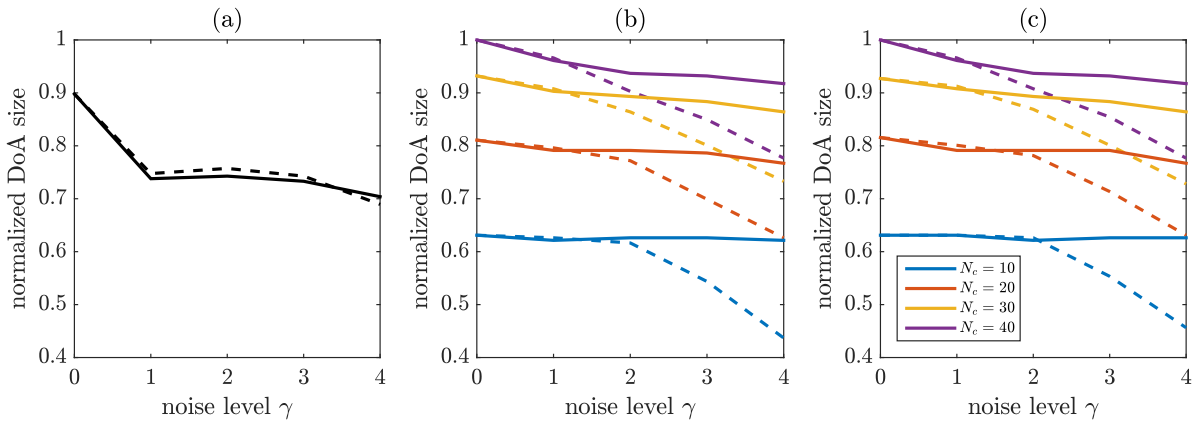

Fig. 10. Normalized domain of attraction size for varying levels of process and measurement noise, with (solid lines) and without (dashed lines) joint state estimation: (a) CLF-C, (b) regulatory NMPC, (c) economic NMPC.

uncertainty decreases size of the domains of attraction, increasing prediction horizon of the MPCs and/or using state estimation jointly with the controllers can be used to alleviate the adverse effects of the uncertainty. Future research could include comparisons with other feedback perimeter control methods and dealing with uncertainty using robust MPC formulations.

Declaration of competing interest

The authors declare that they have no known competing financial interests or personal relationships that could have appeared to influence the work reported in this paper.

Acknowledgment

This research is partially supported by the Swiss National Science Foundation (SNSF) under National Centre of Competence in Research, Dependable Ubiquitous Automation (NCCR Automation), grant agreement 51NF40_180545.

References

Aalipour, A., Kebriaei, H., & Ramezani, M. (2018). Analytical optimal solution of perimeter traffic flow control based on mfd dynamics: A pontryagin's maximum principle approach. *IEEE Transactions on Intelligent Transportation Systems*, *20*(9), 3224–3234. http://dx.doi.org/10.1109/TITS.2018.2873104.

Aboudolas, K., & Geroliminis, N. (2013). Perimeter and boundary flow control in multi-reservoir heterogeneous networks. *Transportation Research, Part B (Methodological)*, *55*, 265–281. http://dx.doi.org/10.1016/j.trb.2013.07.003.

Aboudolas, K., Papageorgiou, M., Kouvelas, A., & Kosmatopoulos, E. (2010). A rolling-horizon quadratic-programming approach to the signal control problem in large-scale congested urban road networks. *Transportation Research Part C (Emerging Technologies)*, *18*(5), 680–694. http://dx.doi.org/10.1016/j.trc.2009.06.003.

Agrawal, A., & Sreenath, K. (2017). Discrete control barrier functions for safety-critical control of discrete systems with application to bipedal robot navigation. In *Robotics: Science and systems*. http://roboticsproceedings.org/rss13/p73.pdf.

Ampountolas, K., Zheng, N., & Geroliminis, N. (2017). Macroscopic modelling and robust control of bi-modal multi-region urban road networks. *Transportation Research, Part B (Methodological)*, *104*, 616–637. http://dx.doi.org/10.1016/j.trb.2017.05.007.

Amrit, R., Rawlings, J. B., & Angeli, D. (2011). Economic optimization using model predictive control with a terminal cost. *Annual Reviews in Control*, *35*(2), 178–186. http://dx.doi.org/10.1016/j.arcontrol.2011.10.011.

Arnott, R. (2013). A bathtub model of downtown traffic congestion. *Journal of Urban Economics*, *76*, 110–121. http://dx.doi.org/10.1016/j.jue.2013.01.001.

Batista, S. F., & Leclercq, L. (2019). Regional dynamic traffic assignment framework for macroscopic fundamental diagram multi-regions models. *Transportation Science*, *53*(6), 1563–1590. http://dx.doi.org/10.1287/trsc.2019.0921.

Bellemans, T., De Schutter, B., & De Moor, B. (2006). Model predictive control for ramp metering of motorway traffic: A case study. *Control Engineering Practice*, *14*(7), 757–767. http://dx.doi.org/10.1016/j.conengprac.2005.03.010.

Bitmead, R. R., Gevers, M., & Wertz, V. (1990). *Adaptive optimal control — The thinking man's GPC*. Prentice Hall New York.

Cannon, M., Deshmukh, V., & Kouvaritakis, B. (2003). Nonlinear model predictive control with polytopic invariant sets. *Automatica*, *39*(8), 1487–1494. http://dx.doi.org/10.1016/S0005-1098(03)00128-6.

Chen, H., & Allgöwer, F. (1998). A quasi-infinite horizon nonlinear model predictive control scheme with guaranteed stability. *Automatica*, *34*(10), 1205–1217. http://dx.doi.org/10.1016/S0005-1098(98)00073-9.

Chen, W.-H., O'Reilly, J., & Ballance, D. J. (2003). On the terminal region of model predictive control for non-linear systems with input/state constraints. *International journal of adaptive control and signal processing*, *17*(3), 195–207. http://dx.doi.org/10.1002/acs.731.

Csikós, A., Charalambous, T., Farhadi, H., Kulcsár, B., & Wymeersch, H. (2017). Network traffic flow optimization under performance constraints. *Transportation Research Part C (Emerging Technologies)*, *83*, 120–133. http://dx.doi.org/10.1016/j.trc.2017.08.002.

Daganzo, C. F. (2007). Urban gridlock: Macroscopic modeling and mitigation approaches. *Transportation Research, Part B (Methodological)*, *41*(1), 49–62. http://dx.doi.org/10.1016/j.trb.2006.03.001.

Daganzo, C. F., & Lehe, L. J. (2015). Distance-dependent congestion pricing for downtown zones. *Transportation Research, Part B (Methodological)*, *75*, 89–99. http://dx.doi.org/10.1016/j.trb.2015.02.010.

Diakaki, C., Papageorgiou, M., & Aboudolas, K. (2002). A multivariable regulator approach to traffic-responsive network-wide signal control. *Control Engineering Practice*, *10*(2), 183–195. http://dx.doi.org/10.1016/S0967-0661(01)00121-6.

Diehl, M., Ferreau, H. J., & Haverbeke, N. (2009). Efficient numerical methods for nonlinear MPC and moving horizon estimation. In L. Magni, D. M. Raimondo, & F. Allgöwer (Eds.), *Nonlinear model predictive control: towards new challenging applications* (pp. 391–417). Berlin, Heidelberg: Springer Berlin Heidelberg, http://dx.doi.org/10.1007/978-3-642-01094-1{_}32.

Ding, H., Zhang, Y., Zheng, X., Yuan, H., & Zhang, W. (2017). Hybrid perimeter control for two-region urban cities with different states. *IEEE Transactions on Control Systems Technology*, *26*(6), 2049–2062. http://dx.doi.org/10.1109/TCST.2017.2746061.

Dotoli, M., Fanti, M. P., & Meloni, C. (2006). A signal timing plan formulation for urban traffic control. *Control Engineering Practice*, *14*(11), 1297–1311. http://dx.doi.org/10.1016/j.conengprac.2005.06.013.

Fu, H., Liu, N., & Hu, G. (2017). Hierarchical perimeter control with guaranteed stability for dynamically coupled heterogeneous urban traffic. *Transportation Research Part C (Emerging Technologies)*, *83*, 18–38. http://dx.doi.org/10.1016/j.trc.2017.07.007.

Fu, H., Wang, Y., Tang, X., Zheng, N., & Geroliminis, N. (2020). Empirical analysis of large-scale multimodal traffic with multi-sensor data. *Transportation Research Part C (Emerging Technologies)*, *118*, Article 102725. http://dx.doi.org/10.1016/j.trc.2020.102725.

Galloway, K., Sreenath, K., Ames, A. D., & Grizzle, J. W. (2015). Torque saturation in bipedal robotic walking through control Lyapunov function-based quadratic programs. *IEEE Access*, *3*, 323–332. http://dx.doi.org/10.1109/ACCESS.2015.2419630.

Geroliminis, N., & Daganzo, C. F. (2008). Existence of urban-scale macroscopic fundamental diagrams: Some experimental findings. *Transportation Research, Part B (Methodological)*, *42*(9), 759–770. http://dx.doi.org/10.1016/j.trb.2008.02.002.

Geroliminis, N., Haddad, J., & Ramezani, M. (2013). Optimal perimeter control for two urban regions with macroscopic fundamental diagrams: A model predictive approach. *IEEE Transactions on Intelligent Transportation Systems*, *14*(1), 348–359. http://dx.doi.org/10.1109/TITS.2012.2216877.

Geroliminis, N., & Sun, J. (2011). Properties of a well-defined macroscopic fundamental diagram for urban traffic. *Transportation Research, Part B (Methodological)*, *45*(3), 605–617. http://dx.doi.org/10.1016/j.trb.2010.11.004.

Godfrey, J. (1969). The mechanism of a road network. *Traffic Engineering & Control*, *8*(8).

Haddad, J. (2015). Robust constrained control of uncertain macroscopic fundamental diagram networks. *Transportation Research Part C (Emerging Technologies)*, *59*, 323–339. http://dx.doi.org/10.1016/j.trc.2015.05.014.

Haddad, J. (2017). Optimal coupled and decoupled perimeter control in one-region cities. *Control Engineering Practice*, *61*, 134–148. http://dx.doi.org/10.1016/j.conengprac.2017.01.010.

Haddad, J. (2017). Optimal perimeter control synthesis for two urban regions with aggregate boundary queue dynamics. *Transportation Research, Part B (Methodological)*, *96*, 1–25. http://dx.doi.org/10.1016/j.trb.2016.10.016.

Haddad, J., & Geroliminis, N. (2012). On the stability of traffic perimeter control in two-region urban cities. *Transportation Research, Part B (Methodological)*, *46*(9), 1159–1176. http://dx.doi.org/10.1016/j.trb.2012.04.004.

Haddad, J., & Mirkin, B. (2016). Adaptive perimeter traffic control of urban road networks based on MFD model with time delays. *International Journal of Robust and Nonlinear Control*, *26*(6), 1267–1285. http://dx.doi.org/10.1002/rnc.3502.

Haddad, J., & Shraiber, A. (2014). Robust perimeter control design for an urban region. *Transportation Research, Part B (Methodological)*, *68*, 315–332. http://dx.doi.org/10.1016/j.trb.2014.06.010.

Haddad, J., & Zheng, Z. (2018). Adaptive perimeter control for multi-region accumulation-based models with state delays. *Transportation Research, Part B (Methodological)*, *137*, 133–153. http://dx.doi.org/10.1016/j.trb.2018.05.019.

Huang, C., Zheng, N., & Zhang, J. (2019). Investigation of bimodal macroscopic fundamental diagrams in large-scale urban networks: Empirical study with GPS data for shenzhen city. *Transportation Research Record*, *2673*(6), 114–128. http://dx.doi.org/10.1177/0361198119843472.

Ingole, D., Mariotte, G., & Leclercq, L. (2020). Perimeter gating control and citywide dynamic user equilibrium: a macroscopic modeling framework. *Transportation Research Part C: Emerging Technologies*, *111*, 22–49. http://dx.doi.org/10.1016/j.trc.2019.11.016.

Ioslovich, I., Haddad, J., Gutman, P.-O., & Mahalel, D. (2011). Optimal traffic control synthesis for an isolated intersection. *Control Engineering Practice*, *19*(8), 900–911. http://dx.doi.org/10.1016/j.conengprac.2011.05.004.

Johansen, T. A. (2000). Computation of Lyapunov functions for smooth nonlinear systems using convex optimization. *Automatica*, *36*(11), 1617–1626. http://dx.doi.org/10.1016/S0005-1098(00)00088-1.

Keyvan-Ekbatani, M., Kouvelas, A., Papamichail, I., & Papageorgiou, M. (2012). Exploiting the fundamental diagram of urban networks for feedback-based gating. *Transportation Research, Part B (Methodological)*, *46*(10), 1393–1403. http://dx.doi.org/10.1016/j.trb.2012.06.008.

Keyvan-Ekbatani, M., Papageorgiou, M., & Knoop, V. L. (2015). Controller design for gating traffic control in presence of time-delay in urban road networks. *Transportation Research Part C (Emerging Technologies)*, *59*, 308–322. http://dx.doi.org/10.1016/j.trc.2015.04.031.

Keyvan-Ekbatani, M., Yildirimoglu, M., Geroliminis, N., & Papageorgiou, M. (2015). Multiple concentric gating traffic control in large-scale urban networks. *IEEE Transactions on Intelligent Transportation Systems*, *16*(4), 2141–2154. http://dx.doi.org/10.1109/TITS.2015.2399303.

Kouvelas, A., Lioris, J., Fayazi, S. A., & Varaiya, P. (2014). Maximum pressure controller for stabilizing queues in signalized arterial networks. *Transportation Research Record: Journal of the Transportation Research Board*, *2421*(1), 133–141. http://dx.doi.org/10.3141/2421-15.

Kouvelas, A., Saeedmanesh, M., & Geroliminis, N. (2017). Enhancing model-based feedback perimeter control with data-driven online adaptive optimization. *Transportation Research, Part B (Methodological)*, *96*, 26–45. http://dx.doi.org/10.1016/j.trb.2016.10.011.

Kouvelas, A., Saeedmanesh, M., & Geroliminis, N. (2017). A linear formulation for model predictive perimeter traffic control in cities. *IFAC-PapersOnLine*, *50*(1), 8543–8548. http://dx.doi.org/10.1016/j.ifacol.2017.08.1411.

Lamotte, R., & Geroliminis, N. (2016). The morning commute in urban areas: Insights from theory and simulation. In *Transportation research board 95th annual meeting*. URL https://trid.trb.org/view/1392730.

Lamotte, R., & Geroliminis, N. (2018). The morning commute in urban areas with heterogeneous trip lengths. *Transportation Research, Part B (Methodological)*, *117*, 794–810. http://dx.doi.org/10.1016/j.trb.2017.08.023.

Leclercq, L., & Paipuri, M. (2019). Macroscopic traffic dynamics under fast-varying demand. *Transportation Science*, *53*(6), 1526–1545. http://dx.doi.org/10.1287/trsc.2019.0908.

Lin, S., De Schutter, B., Xi, Y., & Hellendoorn, H. (2011). Fast model predictive control for urban road networks via MILP. *IEEE Transactions on Intelligent Transportation Systems*, *12*(3), 846–856. http://dx.doi.org/10.1109/TITS.2011.2114652.

Loder, A., Ambühl, L., Menendez, M., & Axhausen, K. W. (2019). Understanding traffic capacity of urban networks. *Scientific Reports*, *9*(1), 1–10. http://dx.doi.org/10.1038/s41598-019-51539-5.

Mariotte, G., Leclercq, L., & Laval, J. A. (2017). Macroscopic urban dynamics: Analytical and numerical comparisons of existing models. *Transportation Research, Part B (Methodological)*, *101*, 245–267. http://dx.doi.org/10.1016/j.trb.2017.04.002.

Menelaou, C., Kolios, P., Timotheou, S., Panayiotou, C., & Polycarpou, M. (2017). Controlling road congestion via a low-complexity route reservation approach. *Transportation Research Part C (Emerging Technologies)*, *81*, 118–136. http://dx.doi.org/10.1016/j.trc.2017.05.005.

Menelaou, C., Timotheou, S., Kolios, P., Panayiotou, C. G., & Polycarpou, M. M. (2018). Minimizing traffic congestion through continuous-time route reservations with travel time predictions. *IEEE Transactions on Intelligent Vehicles*, *4*(1), 141–153. http://dx.doi.org/10.1109/TIV.2018.2886684.

Mohajerpoor, R., Saberi, M., Vu, H. L., Garoni, T. M., & Ramezani, M. (2020). H_∞ Robust perimeter flow control in urban networks with partial information feedback. *Transportation Research, Part B (Methodological)*, *137*, 47–73. http://dx.doi.org/10.1016/j.trb.2019.03.010.

Nguyen, H.-N., Gutman, P.-O., Olaru, S., & Hovd, M. (2013). Implicit improved vertex control for uncertain, time-varying linear discrete-time systems with state and control constraints. *Automatica*, *49*(9), 2754–2759. http://dx.doi.org/10.1016/j.automatica.2013.05.007.

Ni, W., & Cassidy, M. (2019). City-wide traffic control: Modeling impacts of cordon queues. *Transportation Research Part C (Emerging Technologies)*, http://dx.doi.org/10.1016/j.trc.2019.04.024.

Paipuri, M., Xu, Y., González, M. C., & Leclercq, L. (2020). Estimating MFDs, trip lengths and path flow distributions in a multi-region setting using mobile phone data. *Transportation Research Part C (Emerging Technologies)*, *118*, Article 102709. http://dx.doi.org/10.1016/j.trc.2020.102709.

Papageorgiou, M., Diakaki, C., Dinopoulou, V., Kotsialos, A., & Wang, Y. (2003). Review of road traffic control strategies. *Proceedings of the IEEE*, *91*(12), 2043–2067. http://dx.doi.org/10.1109/JPROC.2003.819610.

Ramezani, M., Haddad, J., & Geroliminis, N. (2015). Dynamics of heterogeneity in urban networks: Aggregated traffic modeling and hierarchical control. *Transportation Research, Part B (Methodological)*, *74*, 1–19. http://dx.doi.org/10.1016/j.trb.2014.12.010.

Ramezani, M., & Nourinejad, M. (2018). Dynamic modeling and control of taxi services in large-scale urban networks: A macroscopic approach. *Transportation Research Part C (Emerging Technologies)*, *94*, 203–219. http://dx.doi.org/10.1016/j.trc.2017.08.011.

Rawlings, J. B., & Amrit, R. (2009). Optimizing process economic performance using model predictive control. In L. Magni, D. M. Raimondo, & F. Allgöwer (Eds.), *Nonlinear model predictive control: towards new challenging applications* (pp. 119–138). Berlin, Heidelberg: Springer Berlin Heidelberg, http://dx.doi.org/10.1007/978-3-642-01094-1{_}10.

Rubin, D., Mercader, P., Gutman, P.-O., Nguyen, H.-N., & Bemporad, A. (2020). Interpolation based predictive control by ellipsoidal invariant sets. *IFAC Journal of Systems and Control*, *12*, Article 100084. http://dx.doi.org/10.1016/j.ifacsc.2020.100084.

Saeedmanesh, M., & Geroliminis, N. (2016). Clustering of heterogeneous networks with directional flows based on "Snake" similarities. *Transportation Research, Part B (Methodological)*, *91*, 250–269. http://dx.doi.org/10.1016/j.trb.2016.05.008.

Sirmatel, I. I., & Geroliminis, N. (2018). Economic model predictive control of large-scale urban road networks via perimeter control and regional route guidance. *IEEE Transactions on Intelligent Transportation Systems*, *19*(4), 1112–1121. http://dx.doi.org/10.1109/TITS.2017.2716541.

Sirmatel, I. I., & Geroliminis, N. (2019). Nonlinear moving horizon estimation for large-scale urban road networks. *IEEE Transactions on Intelligent Transportation Systems*, http://dx.doi.org/10.1109/TITS.2019.2946324.

Tettamanti, T., Luspay, T., Kulcsar, B., Péni, T., & Varga, I. (2013). Robust control for urban road traffic networks. *IEEE Transactions on Intelligent Transportation Systems*, *15*(1), 385–398. http://dx.doi.org/10.1109/TITS.2013.2281666.

Varaiya, P. (2013). Max pressure control of a network of signalized intersections. *Transportation Research Part C (Emerging Technologies)*, *36*, 177–195. http://dx.doi.org/10.1016/j.trc.2013.08.014.

van de Weg, G. S., Keyvan-Ekbatani, M., Hegyi, A., & Hoogendoorn, S. P. (2019). Linear MPC-based urban traffic control using the link transmission model. *IEEE Transactions on Intelligent Transportation Systems*, http://dx.doi.org/10.1109/TITS.2019.2938795.

Wongpiromsarn, T., Uthaicharoenpong, T., Wang, Y., Frazzoli, E., & Wang, D. (2012). Distributed traffic signal control for maximum network throughput. In *15th IEEE conference on intelligent transportation systems* (pp. 588–595). IEEE, http://dx.doi.org/10.1109/ITSC.2012.6338817.

Yang, K., Zheng, N., & Menendez, M. (2018). Multi-scale perimeter control approach in a connected-vehicle environment. *Transportation Research Part C (Emerging Technologies)*, *94*, 32–49. http://dx.doi.org/10.1016/j.trc.2017.08.014.

Yildirimoglu, M., Sirmatel, I. I., & Geroliminis, N. (2018). Hierarchical control of heterogeneous large-scale urban road networks via path assignment and regional route guidance. *Transportation Research, Part B (Methodological)*, *118*, 106–123. http://dx.doi.org/10.1016/j.trb.2018.10.007.

Zhong, R., Chen, C., Huang, Y., Sumalee, A., Lam, W., & Xu, D. (2018). Robust perimeter control for two urban regions with macroscopic fundamental diagrams: A control-Lyapunov function approach. *Transportation Research, Part B (Methodological)*, *117*, 687–707. http://dx.doi.org/10.1016/j.trb.2017.09.008.

Zhong, R., Huang, Y., Chen, C., Lam, W., Xu, D., & Sumalee, A. (2018). Boundary conditions and behavior of the macroscopic fundamental diagram based network traffic dynamics: A control systems perspective. *Transportation Research, Part B (Methodological)*, *111*, 327–355. http://dx.doi.org/10.1016/j.trb.2018.02.016.

Zhou, Z., De Schutter, B., Lin, S., & Xi, Y. (2017). Two-level hierarchical model-based predictive control for large-scale urban traffic networks. *IEEE Transactions on Control Systems Technology*, *25*(2), 496–508. http://dx.doi.org/10.1109/TCST.2016.2572169.